Application of an unstructured mesh model to the determination of the baroclinic circulation of the Irish Sea

by

Jiuxing Xing, Alan M Davies and J. Eric Jones

National Oceanography Centre

6 Brownlow Street

Liverpool L3 5DA

U.K.

A three dimensional variable mesh finite volume model is used to compute the baroclinic circulation of the Irish Sea during 1995. Tidal forcing was applied along the model's open boundary with meteorological forcing taken from observations. Initial calculations were performed with a variable mesh model that had high resolution in the well mixed near coastal region; a necessary requirement in order to reproduce tides in the region, although offshore in the stratified area the mesh was slightly coarser than that used in earlier finite difference models. Subsequent calculations were performed using an enhanced resolution which is significantly finer than earlier finite difference models in the off shore region which is thermally stratified in summer due to solar heating and low tidal mixing. This produces a cold water bottom dome separated from the well mixed shallow water regions by strong tidal fronts. Calculations show that both model meshes can reproduce the observed major features of the baroclinic circulation of the western Irish Sea, with the coarse mesh model giving comparable results to earlier finite difference models. In the case of the finer mesh model there are sharper horizontal density gradients in the region of the fronts, which show the presence of baroclinic instability and associated small scale variability as observed in satellite images but not found in the coarser mesh model due to lack of resolution. Results from the fine mesh model show significantly more spatial variability comparable to that found in the measurements.

1. Introduction

One of the major challenges in shallow sea oceanography is the long term simulation of seasonal variability in shallow sea regions subject to significant tidal mixing. Such an area of mixing is the Irish Sea off the west coast of Britain. This is predominantly characterised by strong tidal mixing over the majority of the region where water depths are of the order of 50m, and tidal currents are strong, of the order of $70cms^{-1}$. The exception to this picture is the isolated stratified area in the western Irish Sea (Fig 1), where water depths are deeper (over 100m) and tidal currents are much weaker (of order $10cms^{-1}$). This gives rise to a thermally stratified region in the summer when heat input is a maximum and wind mixing is a minimum. In this region during the stratified summer period there is a surface mixed layer which on average is the order of 5 to 15m thickness separated by a thermocline of about 20m thickness from a cold water bottom layer. In this area tidal mixing is too weak, and a cold water bottom dome of about 100km wide is formed, separated from the shallower tidally mixed regions by a front (Hill et al. 1994, Horsburgh et al. 2000 (hereafter H00), Xing and Davies 2001 (hereafter XD01), Horsburgh and Hill 2003 (hereafter HH03)). For a general description of frontal formation in shallow seas the reader is referred to Hill et al. (2008). Once formed the cold water dome is a stable and persistent summer time feature of the region, and recent measurements (Green et al., 2010) suggest that internal tides are generated within the dome. At the end of summer as wind strength increases, internal waves are generated in the dome region (Xing and Davies 2005a, 2006) and these together with wind induced inertial oscillations and mixing (Davies and Xing 2004, 2005) lead to a breakdown of the cold water bottom dome which subsequently reforms in the next spring as wind forcing decreases and thermal input increases. Consequently the timing of the seasonal formation and breakdown of the cold water dome, its position, lateral and vertical extent, and the intensity of the circulation associated with the dome are a critical test of a model's ability to deal with baroclinic circulation in a shallow tidal sea.

Following the early three dimensional pioneering simulations of Heaps (1973), in the Irish Sea, there were a number of three dimensional tidal and storm surge calculations performed by various authors (e.g. Aldridge and Davies 1993, Davies and Jones 1992, Davies and Jones 1996). In addition the storm surge work was extended by Davies and Lawrence (1995), to include wind wave-current interaction. This early three dimensional modelling focused on homogenous conditions, although subsequently the baroclinic motion of the region, in particular the formation of fronts and the cold water bottom dome was modelled by XD01, HH03, Holt and Proctor (2003). In addition a number of process studies were performed by Xing and Davies (2005b) to determine the mechanisms controlling the circulation within the cold water dome and the role of internal waves in the dome region in influencing its breakdown in winter. These calculations were based upon the application of uniform mesh finite difference models, and hence mesh resolution could not be refined in the dome region where higher resolution was required to resolve the lateral fronts associated with the dome. However, recently Jones and Davies (2005) developed an unstructured mesh finite element model of the west coast of Britain (Fig 2a) and used it to determine an accurate tidal distribution in the region. They showed that it was essential to have both high resolution in the near shore domain and allow for "wetting and drying" over the tidal cycle in order to get the correct level of tidal dissipation and hence an accurate tidal distribution. In a subsequent series of calculations, Xing et al (2010) used a finite volume (F.V.) model of the Irish Sea based upon the FVCOM code (Chen et al 2003,2007) to accurately reproduce the M_2, S_2, N_2, O_1, and K_1 tides over the region shown in Fig2a. By this means the model could include the spring-neap tidal cycle and its modification by the N_2, O_1 and K_1 tides.

In this paper, the finite volume model described above, initially using the irregular mesh shown in Fig 2a, (termed the G3AX mesh (Jones and Davies 2005)) is used with open boundary tidal forcing, and meteorological forcing (namely wind and surface heat) to simulate the thermohaline circulation of the Irish Sea for the stratified period of 1995, and model results are compared with measurements and earlier finite difference calculations, namely XD01 and HH03. A brief description of the model with references for detail and form of the calculations are presented in the next section. In subsequent sections model results are shown.

2. Irish Sea Model (IS-FVCOM).

In the present series of calculations a finite volume (F.V.) code, based upon FVCOM was used to solve the three dimensional non-linear primitive equations. The FVCOM code has been very successful in a number of shallow sea applications. Its ability to simulate the circulation on the New England Shelf (Cowles et al. 2008) suggests that it is an ideal tool for studying the seasonal circulation of the Irish Sea. As details of FVCOM are available in the literature (Chen et al., 2003, 2007, Huang et al., 2008), only a brief summary will be given here. The model is configured to study the baroclinic circulation of the Irish Sea (IS) and part of the Celtic Sea (Fig 1). The IS_FVCOM system solves the three dimensional non-linear hydrostatic primitive equations on an unstructured mesh in the horizontal using a finite volume approach. In the vertical a terrain following sigma (σ) coordinate, or modified s-coordinate is used. In the present calculations 27 sigma levels were used in the vertical, with enhanced resolution in the surface and bottom boundary layers. Vertical mixing was computed using a two equation Mellor-Yamada turbulence energy closure model which contains predictive equations for the turbulence energy q^2, and mixing length l. In order to take account of an enhanced source of turbulence in the surface layer due to wave breaking, a Craig and Banner (1994) surface boundary condition for q^2, was used. As shown by Mellor and Blumberg (2004)(hereafter denoted MB) and Stacey (1999), the inclusion of a wave dependent source of turbulence energy and associated modification of the mixing length (l) improved the accuracy of the

Mellor-Yamada model. As discussed in MB, the form of the mixing length l is important in determining mixed layer depth, and temperature distribution within it. Based on observations (see MB for detail), various formulations of l are appropriate, namely

$$l = K z_w + l_m \qquad (1)$$

With K=0.4 Von Karman coefficient, z_w a wave induced mixing length, and l_m, the mixing length computed with the Mellor-Yamada model.

In the case of wave induced turbulence due to breaking waves, the surface mixing length is difficult to determine as is its vertical variation (see MB for a detailed discussion). For simplicity an exponentially decaying wave induced mixing length was assumed of the form

$$Z_w = H_s e^{-Z_p / H_s} \qquad (2)$$

with $Z_p = \max(0, z - \lambda H_s)$, (3)

and z the distance below sea surface, H_s significant wave height, with λ an arbitrary coefficient determining the depth of mixing due to wind waves. In essence if λ=4, wave turbulent mixing is assumed to penetrate to the order of $4H_s$, (with H_s the significant wave height) as found in the bubble observations of Thorpe (1984, 1992). The mixing length used in the F.V. model was then given by equation (1), with l_m determined from the Mellor-Yamada turbulence closure scheme.

For temperature a derivative surface boundary condition as in XD01 was applied at the surface, namely

$$K_h \frac{\partial T}{H \partial \sigma} = \frac{Q}{C_p \rho_o} \qquad (3)$$

with K_h vertical diffusion coefficient, H water depth, T temperature, C_p the specific heat capacity of seawater and Q the net heat flux, calculated from

$$Q = Q_s + K_q (T_d - T_s) \qquad (4)$$

where Q_s is the observed surface insolation; T_s is the modelled sea surface temperature; T_d is the dewpoint temperature; and K_q is the heat loss coefficient, which is a function of wind speed. The term $K_q(T_d\text{-}T_s)$ includes all heat loss mechanisms (e.g. evaporation, infrared back radiation) and heat gain at the sea surface. In essence the meteorological forcing in the model was identical to that used by XD01, although the parameterization of vertical mixing was slightly different, in particular the form of the vertical mixing length that included wave mixing as discussed previously.

The prognostic equation for temperature evolution contains the vertical derivative of the shortwave solar insulation I(ms^{-1}K) which is given by a double exponential function following Paulson and Simpson (1977), thus

$$I = \frac{Q_s}{c_p \rho_o}\left(\alpha e^{\frac{\sigma H}{\lambda_1}} + (1-\alpha)\alpha e^{\frac{\sigma H}{\lambda_2}}\right) \qquad (5)$$

with α a constant taken as 0.62, and λ_1 and λ_2 are extinction depths (we use λ_1=1.5m and λ_2=20m); σ vertical coordinate (0 at sea surface and -1 at seabed).

At the sea bed a quadratic bottom friction law was used as in Chen et al (2003, 2007). As in Chen et al (2003, 2007), the Smagorinsky form of horizontal viscosity (with a coefficient of 0.2) was used in the model, although the horizontal diffusion of temperature was neglected. This term was omitted because preliminary calculations showed that it gave rise to a spurious increase in bottom temperatures within the cold water dome due to lateral diffusion from the warmer shallow regions.

3. Numerical Calculations

In order to examine to what extent mesh variability over the Irish Sea, in particular in the dome region, influenced the circulation in the western Irish Sea, calculations were performed with two different meshes. The first (mesh G3AX, Fig 2a) is identical to that used by Jones and Davies (2005) in an accurate simulation of the tide and has enhanced resolution in the near shore regions in order to accurately dissipate tidal energy in these areas and hence reproduce the tide over the whole domain. Although this model could accurately reproduce the tide in the area, the model's mesh is not sufficiently fine (of order 5km in the dome region) to resolve the high density gradients and circulation associated with the cold water dome in the western Irish Sea. To improve resolution in this region, the mesh was enhanced locally giving mesh G3AXWL (Fig 2b) which was identical to G3AX except for a local refinement in the dome region, where the mesh sizes were less than 1km.

In all calculations the model meshes are based on the same water depths and coastline. All calculations have the same open boundary M_2 tidal forcing taken from Xing et al (2010). The meteorological forcing was hourly values of wind stress, net incoming solar heating, and the long wave heat flux at the sea surface as described previously. Values of wind speed and direction, shortwave component of surface isolation, and dewpoint temperature were obtained from the Dublin Airport station as in XD01. By this means model results could be compared with XD01, although that model was confined to just the Irish Sea, namely from about 55°N to 52°N and had a resolution of approximately 3.6km by 3.0km (see XD01) for detail. To be consistent with previous finite difference calculations (XD01, HH03), spatially uniform meteorological forcing was applied. The difficulty of applying spatially uniform meteorological forcing was that up-/down-welling produced by divergences or convergences in the wind stress that could influence vertical mixing and flow fields were not included. However, as the main focus here is to examine the sensitivity of the solution to mesh resolution and compare with earlier finite difference calculations, then uniform meteorological forcing is justified.

To be consistent with XD01, and make comparisons with the finite difference model of HH03 (which covered an identical region to XD01), and measurements taken by H00, the meteorological forcing from 1995, was used in the calculation. The summer months of 1995 were unusually warm, and also there was a sea surface temperature satellite image available for comparison purposes. The same image was used by XD01. All calculations were started from a homogenous sea region with an initial temperature of 7.5°C, and integrated forward in time from the 21/March (Year Day 80, Model Day 1) until 31/October (Year Day 304), as in HH03. Although the main focus of the present study is the Irish Sea, the larger region covered by the model will be examined when measurements are available outside the Irish Sea region, such as occurred in the satellite image of 26/June/95 (Fig 3).

3.1. Temperature and circulation on 26/June/95

3.1.1. Solution using coarse mesh G3AX.

Considering initially the temperature distribution on 26/June/95, derived from the satellite. A dominant feature of the satellite image is the cold water band that extends from the south west of the Isle of Man down into the Celtic Sea. This corresponds to the deep water region of reduced mixing that separates the stratified region to the west of the Isle of Man from the shallow well mixed tidal water of the eastern Irish Sea. The location of this cool water band, and the warmer surface waters of the western Irish Sea associated with the dome region are well reproduced by the model (Fig 4a), as are the warmer waters of the eastern Irish Sea. The increased surface temperature (T_s) of the Celtic Sea water found in the satellite image also occurs in the model, as does the decrease in surface temperature through the North Channel, and in the area just to the north of it. In this region the tidal currents are strong, giving rise to enhanced vertical mixing. However, just to the north west of this where tidal currents are reduced, both model and observations show an increase in surface temperature associated with reduced vertical mixing. Bottom temperature (T_b) contours (Fig 4b) and differences in surface and bed temperatures (T_s-T_b)(Fig 4c), clearly reveal the presence of a cold water bottom dome in the western Irish Sea. In addition in the eastern Irish Sea between the Isle of Man and the coast there is a region of weak vertical stratification corresponding to an area of diminished (currents of order 10cms^{-1}) tidal flow. Both the strongly stratified western Irish Sea region and the weaker area in the eastern Irish Sea (see "blow ups", Figs 5a,b,c) are found in other models (e.g. XD01 and HH03) and in observations (H00).

Although the spatial distribution of the surface temperature field computed with the model is in good agreement with the satellite image, it is evident that some of the observed small scale frontal features, possibly due to baroclinic instability, are not resolved with the model. To examine these in more detail in the western Irish Sea, plots of the density driven flow at sea surface and seabed were computed using solutions based on meshes G3AX and G3AXWL (see later discussion). The density driven flow corresponding to the temperature distribution at a given time was separated from the total flow due to density, wind and tide, by running the model for two days with the appropriate temperature field but without tidal and meteorological forcing. By this means the tidal and wind driven currents were removed together with any tidal advection effects (see later). Contours of surface and bottom temperature fields, and corresponding currents (note scale differences between surface and bottom currents) computed using mesh G3AX are shown in Figs 6(a) and (b). It is evident that there is a cyclonic gyre at sea surface in the western Irish Sea as predicted by simple geostrophic theory (Hill 1996, Xing and Davies 2005b, Davies and Xing 2006). However the bed current (Fig 6b) exhibits significantly larger spatial variability possibly due to an ageostrophic component of the current.

A cross section through the dome at 53.8°N shows (Fig 7a) a strong near surface thermocline, with the top of the dome located at about 20m below the surface. Below this layer, intense bottom mixing significantly reduces the vertical density gradient, with lateral differential mixing giving rise to horizontal temperature gradients in the sea bed region. Associated with this temperature distribution the v velocity field shows an anticlockwise (cyclonic) circulation in the upper part of the water column, with reduced bottom currents in the opposite direction on the east side of the dome. The u velocity field only exhibits an appreciable flow on the east side of the dome, although it is clear from Fig 6(a)(b) that this cross sectional flow field depends upon where the cross section is taken within the dome. The vertical velocity distribution (Fig 7a) exhibits some upwelling on the western side of the dome, with downwelling within the centre, and an indication of upwelling on its eastern edge. These flow fields in the western Irish Sea, and cross sectional plots are in good agreement with the earlier modelling work of XD01 (see their Figs 8 and 9). However, both their model and the present one, fail to resolve the small scale features found in the satellite image associated with baroclinic instability in the frontal region. To examine this in more detail identical calculations were performed with the higher resolution model.

3.1.2 Solutions using the fine resolution G3AXWL mesh.

Comparing “blow ups” of surface (T_s), bottom (T_b) and differences (T_s-T_b) temperatures in the Irish Sea between those computed with mesh G3AX (Figs 5(a)-(c)) with those derived using mesh G3AXWL (Figs 5d-f) it is evident that both solutions exhibit the same large scale features. However, in the case of the higher resolution model there are significantly more fine scale features in the temperature field, in particular for the surface temperature distribution in the frontal region associated with the dome. In this respect the solution computed with the finer mesh is in better agreement with the satellite image than that computed with the coarse mesh model.

In order to compare the large scale features of the flow field, it is valuable to output those computed on the fine mesh onto a coarser mesh (Fig 6(c)(d)), although the temperature contours are based on the fine mesh. Jones and Davies (2007) used a similar method to look at different space scales in tidal residuals. Comparing surface currents derived with coarse and fine meshes (Figs 6(a) and 6(c)) it is evident that the large scale cyclonic circulation around the dome is found in both calculations. However the intensity of the currents particularly in some of the lateral boundary layers along the east coast of Ireland and west coast of the Isle of Man are stronger in the higher than lower resolution model. This reflects the ability of the finer mesh to resolve sharp horizontal temperature gradients and the resulting near geostrophic flows. In addition in the finer mesh model in the south western part of the dome near 53.5°N, -5.3°W (Fig 6c) there are some strong frontal features with associated baroclinic instability which are resolved in the higher mesh model. In proximity to these fronts there are strong local flows (Fig 6c) on the fine but not on the coarser mesh solution (Fig 6a). Similar features are found in the bottom currents (compare Figs 6b and 6d). Again both models exhibit similar large scale flows although there are differences on the small scale and in the intensity of local horizontal temperature gradients.

It is evident from the fully resolved surface current flow field on the fine mesh (Fig 6e), in a subdomain of the model centred on the region of significant baroclinic instability, that there is appreciable small scale variability in the currents. These reflect the rapid changes in density field associated with baroclinic instability which to a certain extent mask the large scale flow associated with the dome. However by interpolating the flow field to a coarser mesh (Fig 6c,d) while retaining the details of the temperature field it is possible to determine the dome's large scale circulation. Also the details of the temperature field are comparable to those found in the satellite image. A similar complex spatial distribution of bottom currents (not shown) was also found.

At present a detailed validation of these highly spatially variable temperature and current fields is very difficult to accomplish. This is because the temperature field is measured by towing probes that "see-saw" in the vertical behind a ship (see H00) and hence a synoptic data set is not obtained, and at best a cross section over a few days is only possible (see later discussion). In addition it is not possible to accurately remove tidal advection effects from these observed temperature fields. For currents, very limited point current measurements are available and those obtained by drogues (H00) measure the total current namely tide, wind and density from which it is difficult to separate out the density driven circulation. In addition these are not fixed point measurements as in the model, but are Lagrangian measurements and hence all small scale motion that cannot be resolved in the model, contributes to the drogues motion. This makes comparisons with model flows particularly difficult. In terms of surface temperatures and currents, the comparison with the satellite image suggests that the small scale frontal features are real, although without high resolution H.F. Radar current distributions (e.g. Davies et al 2001a,b), validation of surface current fields is not possible.

Despite these difficulties in model validation, and the presence of small scale changes in the temperature and current field produced by baroclinic instability, it is valuable to compare cross section solutions from the high resolution model with those from the coarser mesh solution (Figs 7a and 7b). Considering initially the cross section temperature field through the centre of the dome. It is evident from Figs 7a and 7b, that the large scale features are comparable, although the higher resolution model shows more small scale variability, with a depression of the temperature surface at -5.2°W, that is not found in the coarser solution. This is associated with the region of rapidly changing v velocity in this area (Fig 7b), due to local baroclinic instability, with the v velocity changing direction over a distance of a few kilometres. This small scale change can be resolved on the high resolution mesh (Fig 7b) but not the coarser mesh (Fig 7a). In addition there are comparable rapid changes in the u component of velocity (Fig 7b) that were not found previously (Fig 7a). Associated with these divergences/convergences in the u and v velocity fields are regions of upwelling/downwelling vertical velocity which are responsible for the local upwelling/downwelling of the temperature field in the high resolution model (Fig 7b). In terms of the bottom front in the dome region, it is apparent that the horizontal temperature gradient in the fine mesh model (Fig 7b) at about -5.2°W is significantly sharper than in the coarse mesh model (Fig 7a) due to enhanced resolution.

To examine to what extent these small scale effects are persistent features, how temperature distribution varies over the year, and compare model solutions with those of HH03 and observations H00, three periods when cross section measurements are available were also examined, namely 25/July (model day 126), 16 August (model day 148) and 21 September (model day 184).

3.2 Temperature distribution on 25/July/95.

Surface (T_s), bottom (T_b) and differences (T_s-T_b) computed with both the coarse (Figs 8a-c) and fine mesh models (Fig 8d-f) on 25/July/95 show comparable distributions to those computed by HH03, and are in good agreement with observations (H00). As previously the major difference between the two solutions is the presence of the small frontal features on the high resolution model which are absent in the coarse mesh model and that of HH03. The model of HH03 had an identical resolution to XD01, namely 1/20° of longitude and 1/30° of latitude, giving a uniform finite difference grid of 3.3km by 3.7km. A consequence of this coarse horizontal mesh was that neither the model of XD01, or HH03 could resolve the frontal instability features shown here in the high resolution model.

Comparison of temperature fields along cross section 53° 40’N (near the centre of the dome) (Fig 9a,b) shows that as previously (Figs 7a,b) there is more small scale spatial variability in the fine mesh temperature field (Fig 9b) than that computed with the coarser mesh model (Fig 9a). In addition, as previously the bottom front at about -5.3°W is much sharper in the fine mesh model (Fig 9b) than coarse mesh (Fig 9a) due to enhanced resolution. The coarse mesh solution (Fig 9a) is in close agreement with the solution of HH03 (see Fig 12b in HH03), with both models having a near surface temperature of 16.5°C in good agreement with observations (see Fig 12a in HH03). However the near bed temperature in HH03 is about 11.5°C in the centre of the dome (see Fig 12b in HH03) whereas in the present model it is below 10°C which is in good agreement with the observed value (see Fig 12a in HH03). In addition the observations show more small scale variability than found in the present coarse mesh model or the model of HH03. However the observed spatial variability is less than that found in the high resolution model (Fig 9b). In addition the observations do not show the well mixed region between -5.2°W and -5°W below the 13°C isotherm shown in Fig 9b, nor the strong horizontal gradient in this region shown in Fig 9a and also found by HH03. In this area the observations suggest weak vertical and horizontal gradients, which are not reproduced by any model. This suggests that perhaps the horizontal mixing is too large in the fine mesh model, and under-resolved in the coarser mesh models. However, as discussed previously, unlike model solutions which are at a given time, the observations are based upon measurements from an instrument towed behind a ship which “see-saws” in the vertical, and are not synoptic. In fact it takes several days for the ship to cross the dome, during which mixing and tidal advection play a role. This will obviously influence the accuracy of measurement-model intercomparisons. Despite these problems it is useful to examine how the temperature distribution varies with time. To this end comparisons were also made on the 16/Aug and 21/Sept.

3.3 Temperature and circulation on 16/Aug/95

As previously temperature distributions on the 16/Aug/95 computed with the high resolution model exhibit significantly more small scale variability in the frontal region of the dome (Figs 10d-f) than in the coarse mesh solution (Figs 10a-c). At this time of the year the large scale horizontal temperature gradient in the dome region is greater than previously (namely 26/June) and gives rise to a stronger cyclone surface circulation in the high resolution than coarser resolution model (compare Figs 11a and 11b, noting differences in vector scales) in the surface layer. Stronger currents were also found in the near bed region (not shown). The distribution of surface currents from the coarse mesh model (Fig 11a) in the dome region is in close agreement with the model results presented in HH03 (see Fig 9b in that paper). However in coastal regions the currents computed with the variable mesh model are significantly stronger due to the ability of the present model to resolve the near shore region. In addition as shown by Aldridge and Davies (1993), the “stair case” nature of the finite difference grid in the coastal boundary generates a spurious flow over a region of four or five grid boxes adjacent to the coast in a uniform finite difference model.

As shown earlier (Fig 6e) the high resolution model gives rise to rapidly varying currents (not presented) in regions of strong frontal instability such as those shown in Figs 10d-f. Even when these currents are output on a coarser mesh (Fig 11b) it is clear, particularly in regions of large horizontal density gradients, and hence potential baroclinic instability, that the large scale circulation associated with the dome is partially masked by these local flow fields (compare Figs 11a and 11b). A major problem with the high resolution solution is how the accuracy of the small scale current and temperature features predicted with the model can be assessed. This will be discussed further later in the paper.

Comparing the temperature cross section along 53°40'N computed with the coarse mesh model (Fig 9c) with that computed by HH03 (see Fig 12d in HH03) it is evident that both models predict a strong surface thermocline. In addition below a depth of 20m, there is a strong horizontal temperature gradient with the variable mesh model giving a bottom temperature in the centre of the dome of about 11°C compared to 11.5°C in the HH03 calculation. A detailed comparison of solutions showed that on average the coarse mesh model gave temperatures about 0.5°C higher than those computed by HH03, with no significant differences in the horizontal and vertical distribution of the isotherms. However the distribution of isotherms based on measurements (Fig 12c in HH03) showed much weaker horizontal and vertical density gradients particularly on the eastern side of the dome than found in these models. These measurements tended to support the weaker horizontal and vertical density distribution on the east side of the dome shown in Fig 9d rather than those given in Fig 9c. In addition the strong near surface thermocline found on the eastern side of the dome (Fig 9d), and the weaker horizontal density gradient in this region at depth shown in Fig 9d was also supported by the measurements. This again suggests that the coarse mesh model and the comparable resolution finite difference models (e.g. XD01, HH03) are underpredicting the across frontal mixing in these regions, due to a lack of horizontal resolution.

3.4 Temperature distributions on 21/Sept/95.

To determine to what extent the solutions differ at a time of autumn cooling, temperature distributions computed with both the coarse (Figs 12a-c) and fine (Fig 12d-f) meshes were determined. At this time the surface temperature field computed with the coarse mesh model (Fig 12a-c) showed little spatial variability compared with earlier times, although the bottom temperature distribution and (T_s-T_b) contours showed the presence of a cold water bottom dome. In the case of the higher resolution model, as earlier in the year the spatial distribution was comparable to that found with the coarser mesh model, although small scale features, particularly in the near bed temperatures were evident (Fig 12e).

As previously the temperature cross section computed with the coarse mesh model (Fig 9e) exhibits a uniform bottom dome like feature with none of the small scale ripples found in the higher resolution solution, which has a tendency to be warmer on the easterly than westerly side. This asymmetry was found by HH03, and in the observations which tended to show weak vertical temperature gradients on either side of the dome. This suggests that the tidal and wind mixing in the shallow regions on either side of the dome may be too strong.

To finalise the comparison of temperatures computed with the different meshes, time series of surface and bottom temperatures from the centre of the stratified region namely 53.8°N, 5.5°W were plotted and compared to observed near surface (circles) and near bed (diamonds) temperatures (Figs 13a,b). Also plotted were computed vertical temperature profiles. Both solutions show significant time variability in the surface temperature signal which is modulated by short term variations in solar input and wind stress. Bottom temperatures show a much smoother time variation reflecting the isolation of the bottom boundary from short term variations in the meteorological forcing. Both model solutions show good agreement with measurements, with the coarser mesh model given slightly (of order 0.2°C) warmer surface and bottom temperatures than the fine mesh model. This is possibly due to slightly larger mixing in the fine mesh model. The most significant difference between the models is in the vertical temperature profiles, which exhibit smaller scale variability in both the vertical and with time in the finer than coarse mesh. This is to be expected since as shown earlier there is significantly more spatial variability in the temperature and current fields computed with the fine than coarse mesh. The time series plots were comparable to those computed with HH03 using their uniform grid finite difference model.

These intercomparisons suggest that in terms of the large scale features of the dome circulation, and its temperature distribution these can be adequately resolved using uniform mesh models with resolutions of the order of 3km (e.g. the models of XD01 and HH03). In addition the unstructured coarse mesh model used here can adequately resolve the dome region, with the added advantage of giving high resolution in the coastal boundary layer where currents show local enhancements. In terms of a detailed description of the frontal dynamics of the dome region, this requires the application of a fine mesh model.

4. Concluding Remarks

A variable mesh finite volume model was used to examine the influence of mesh resolution upon the accuracy of the computed baroclinic motion of the Irish Sea. Initial calculations were performed using a mesh designed to reproduce tides in the region (namely mesh G3AX) rather than to resolve the dynamics of the cold water dome in the western Irish Sea, where the mesh is relatively coarse. In this coarse mesh model, the resolution was refined in the near coastal zone, where tides are largest, and consequently there is maximum tidal mixing and loss of tidal energy. Calculations with this model showed that it could reproduce the M_2, S_2, N_2, K_1 and O_1 tides together with their higher harmonics (Xing et al 2010). Although this model can reproduce a range of tidal constituents, as shown by other authors (e.g. XD01, HH03) it is only necessary to include the M_2 tide in order to get an adequate description of the tidal mixing in the region, and the baroclinic circulation. To this end the model was forced with the M_2 tide, and identical meteorological forcing as used in XD01 in simulating the 1995 annual circulation. This year was chosen because solutions were available from two uniform finite difference models of the Irish Sea, namely XD01 and HH03, with which comparisons could be made, and also some observational data (H00) was available for comparison. Although the meteorological data was identical to that used in XD01, a slightly different turbulence closure model was applied in the vertical. Hence in the present models a two equation closure scheme was applied in the vertical with a surface source of wave turbulence and a surface wave dependant mixing length.

Comparison of solutions computed with the coarse mesh model, with uniform finite difference models (XD01, HH03) and observations showed that the model could reproduce the large scale features of the baroclinic circulation in the dome region together with the associated temperature field. Comparison with the surface temperature measured with a satellite revealed that it could not reproduce the small scale frontal instability shown on the satellite image. Subsequent calculations using a fine mesh model based upon the mesh resolution G3AX, but with the mesh refined in the region of the dome (namely G3AXWL) showed that this model could resolve the fine scale temperature features in the frontal region of the dome. However there were no measurements available to determine how accurately the model could reproduce these small scale features. In addition a simulation of these small scale effects would require a detailed determination of the meteorological forcing over the region that was not available.

Comparing cross sectional distributions of temperature computed with both meshes with observations (HH03, H00) showed that those derived with the higher resolution model tended to be in better agreement with observations. Also computed temperature fields derived with the higher resolution model showed small scale spatial features that were found in the observations. In addition the computed bottom density front in this model was significantly sharper than that found in the coarse mesh model. This suggested that the small scale frontal processes could be resolved in this model but not in the coarser mesh model.

Although a rigorous validation of the small scale frontal features of the high resolution model could not be performed, this model has the potential to be able to simulate the recently observed internal tides found in the western Irish Sea (Green et al 2010) since the mesh resolution is particularly high in this area. In addition since the mesh resolution is high in the near coastal region, the model has the potential to accurately resolve the regions of fresh water influence and the associated tidal mixing. Calculations to investigate these processes are presently in progress.

Acknowledgements

The authors are indebted to FVCOM group for making their code available for us, Phil Hall for assistance on cluster, E. Ashton for typing the paper and R. Smith for help in figure preparation.

References

Aldridge, J. N. and Davies, A.M (1993) A high resolution three-dimensional hydrographic tidal model of the eastern Irish Sea. Journal of Physical Oceanography, 23, 207-224.

Chen, C., Huang, H., Beardsley, R.C., Liu, H., Xu, Q., Cowles, G. (2007) A finite volume numerical approach for coastal ocean circulation studies: Comparisons with finite difference models, Journal of Geophysical Research., 112, C03018, doi: 10.1029/2006JC003485

Chen, C., Liu, H., Beardsley, R.C. (2003) An unstructured grid, finite-volume, three-dimensional, primitive equations ocean model: Application to coastal ocean and estuaries. Journal of Atmospheric and Oceanic Technology 20, 159-186.

Cowles, G.W., Lentz, S.J., Chen, C., Xu, Q. and Beardsley, R.C. (2008) Comparison of observed and model-computed low frequency circulation and hydrography on the New England Shelf. Journal of Geophysical Research, 113, C09015 doi: 10.1029/2007JC004394.

Craig, P.D. and Banner, M.L. (1994) Modelling wave-enhanced turbulence in the ocean surface layer. Journal of Physical Oceanography 24, 2546-2559.

Davies, A.M., Hall, P., Howarth, J.M., Knight, P., and Player, R. (2001a) Comparison of observed (HF Radar and ADCP measurements) and computed tides in the North Channel of the Irish Sea, Journal of Physical Oceanography, 31, 1764-1785.

Davies, A.M., Hall, P., Howarth, J.M., Knight, P., and Player, R, (2001b) A detailed comparison of measured and modelled wind driven currents in the North Channel of the Irish Sea, Journal of Geophysical Research, 106, 19,683-19,713.

Davies, A.M. and J.E. Jones (1992) A three dimensional wind driven circulation model of the Celtic and Irish Seas. Continental Shelf Research, 12, 159-188.

Davies, A.M. and J.E. Jones (1996) Sensitivity of tidal bed stress distributions, near bed currents, overtides and tidal residuals to frictional effects in the eastern Irish Sea. Journal of Physical Oceanography 26, 2553-2575.

Davies, A.M. and J. Lawrence (1995) Modelling the effect of wave-current interaction on the three-dimensional wind driven circulation of the eastern Irish Sea. Journal of Physical Oceanography 25, 29-45.

Davies and Xing, J. (2004) Wind induced motion in the vicinity of a bottom density front.: Response to forcing frequency. Journal of Geophysical Research, 109, CO9002, doi:10.1029/2003JC002151

Davies, A.M. and Xing, J. (2005) The effect of a bottom shelf front upon the generation and propagation of near-inertial internal waves in the coastal ocean. Journal of Physical Oceanography (35), 6, 976-990.

Davies, A.M. and Xing, J. (2006) Effect of topography and mixing parameterization upon the circulation in cold water domes. Journal of Geophysical Research, 111, C03018, doi:10.1029/2005JC003066.

Jones, J.E. and A.M. Davies (2005) An intercomparison between finite difference and finite element (TELEMAC) approaches to modelling west coast of Britain tides. Ocean Dynamics 55, 178-198.

Green, J.A.M., J.H. Simpson, S.A. Thorpe, and T.P. Rippeth (2010) Observations of internal tidal waves in the isolated seasonally stratified region of the western Irish Sea. Continental Shelf Research 30, 214-225.

Heaps, N.S. (1973) Three-dimensional numerical model of the Irish Sea. Geophys. J. Roy. Astron. Soc. 35, 99-120.

Hill, A.E., R.Durazo, and D.A.Smeed (1994) Observations of a cyclonic gyre in the western Irish Sea. Continental Shelf Research, 14, 479-490.

Hill, A.E. (1996) Spin-down and the dynamics of dense pool gyres in shallow seas. Journal of Marine Research, 54, 471-486.

Hill, A.E., Brown, J., Fernand, L., Holt, J., Horsburgh, K.J., Proctor, R., Raine, R. and W.R. Turrell (2008) Thermohaline circulation of shallow tidal seas. Geophysical Research Letters, 35, L11605, doi:10.1029/2008GLO33459.

Holt, J.T. and R. Proctor (2003) The role of advection in determining the temperature structure of the Irish Sea. Journal of Physical Oceanography, 33, 2288-2306

Horsburgh, K.J., A.E.Hill, J. Brown, L. Fernand, R.W. Garvine and M.M. P. Angelico (2000) Seasonal evolution of the cold pool gyre in the western Irish Sea. Progress in Oceanography 46, 1-58.

Horsburgh, K.J., and A.E. Hill (2003) A three-dimensional model of density-driven circulation in the Irish Sea. Journal of Physical Oceanography, 33, 343-365.

Huang, H., Chen, C., Blanton, J.O., and Andrade, F.A. (2008) A numerical study of tidal asymmetry in Okatee Creek, South Carolina. Estuarine Coastal and Shelf Science, 78, 190-202.

Jones, J.E. and Davies, A.M. (2007) On the sensitivity of tidal residuals off the west coast of Britain to mesh resolution. Continental Shelf Research, 27, 64-81.

Mellor, G. and Blumberg, A. (2004) Wave breaking and ocean surface layer thermal response. Journal of Physical Oceanography, 34, 693-698.

Paulson, C., and Simpson, J.J. (1977) Irradiance measurements in the upper ocean. Journal of Physical Oceanography 7, 952-956.

Stacey, M.W. (1999) Simulation of the wind-forced near-surface circulation in Knight Inlet: A parameterization of the roughness length. Journal of Physical Oceanography 29, 1363-1367.

Thorpe, S.A. (1984) On the determination of K_v in the near surface ocean from acoustic measurements of bubbles. Journal of Physical Oceanography, 14, 855-863.

Thorpe, S.A. (1992) Bubble clouds and the dynamics of the upper ocean. Quarterly Journal of the Royal Meteorological Society, 118, 1-22.

Xing, J. and Davies, A.M. (2001) A three-dimensional baroclinic model of the Irish Sea: formation of the thermal fronts and associated circulation. Journal of Physical Oceanography, 31, 94-114.

Xing, J. and Davies, A.M. (2005a) Influence of a cold water bottom dome on internal wave trapping. Geophysical Research Letters. 32: L03601, doi:10.1029/2004GL021833.

Xing, J. and Davies, A.M. (2005b) A model study of spin-down and circulation in a cold water dome. Ocean Dynamics, 55, 199-212.

Xing, J. and Davies, A.M. (2006) Internal wave trapping and mixing in a cold water dome, Journal Geophysical Research, 111, C07002, doi:10.1029/2005JC003417.

Xing, J., Davies, A.M. and Jones, J.E. (2010) Computing the M_2, M_4, M_6, S_2, N_2, K_1 and O_1 tides off the west coast of Britain with both a finite volume and finite element approach (submitted).

Figure captions

Fig 1: Topography (in meters) of the region covered by the model and places named in the text.

Fig 2: (a) Finite volume mesh of the west coast of Britain (mesh G3AX) and (b) same mesh but with enhanced resolution in the region of the cold water dome (mesh G3AXWL), (c) expanded plot of a sub-domain of (b) showing mesh change from coarse to fine.

Fig3: Sea surface temperature satellite image at midday 26/June/1995. Dark areas are cloud or land with white line marking the coast.

Fig4: Contours over whole model domain of (a) surface temperature (°C), (b) bottom temperature (°C), (c) surface-bottom temperature difference (°C) on 26/June/1995 computed with mesh G3AX. Note: contour interval (1°C)

Fig 5: As Fig 4, but for the Irish Sea region of the model (contour interval 0.5°C). Computed (a),(b),(c) using mesh G3AX, and (d)(e)(f) using mesh G3AXWL.

Fig 6: Temperature contours (°C, contour interval 0.5°C) and current vectors at (a) sea surface, (b) sea bed (note difference in current scales) over the western Irish Sea computed with mesh G3AX, and (c), (d) using mesh G3AXWL, with vectors output on a coarser mesh, and (e) for a subdomain on every grid, for 26/June/1995. (Note differences in vector scales).

Fig 7: A west-east cross section at 53.8°N of temperature (°C, contour interval 0.5°C), v and u components of velocity (cms^{-1}, contour interval $1cms^{-1}$) and vertical velocity w ($cms^{-1}x10^{-3}$, contour interval $10^{-3}cms^{-1}$) computed using (a) mesh G3AX and (b) mesh G3AXWL on 26/June/1995.

Fig 8: Contours over the Irish Sea region of (a) surface temperature (°C), (b) bottom temperature (°C), (c) surface-bottom temperature difference (°C) on 25/July/1995, computed with mesh G3AX, and (d), (e), (f) computed with mesh G3AXWL.

Fig 9: A west-east cross section at 53.8°N of temperature (°C, contour interval 0.5°C) computed with (a) mesh G3AX, (b) mesh G3AXWL on the 25/July/1995, (c) mesh G3AX, (d) mesh G3AXWL, but on 16/Aug/1995, (e) mesh G3AX, (f) mesh G3AXWL, but on 21/Sept/1995.

Fig 10: Contours over the Irish Sea region of (a) surface temperature (°C), (b) bottom temperature (°C), (c) surface-bottom temperature difference (°C) on 16/Aug/1995 computed with mesh G3AX, and (d), (e), (f) computed with mesh G3AXWL.

Fig 11: Temperature contours (°C, contour interval 0.5°C) and surface current vectors (a) computed on mesh G3AX, (b) computed on mesh G3AXWL, but with output on a coarse mesh, at 16/Aug/1995. (Note differences in vector scales).

Fig 12: Contours over the Irish Sea region of (a) surface temperature (°C), (b) bottom temperature (°C), (c) surface-bottom temperature difference (°C) on 21/Sept/1995 computed with mesh G3AX and (d), (e), (f) computed with mesh G3AXWL.

Fig 13: Time series of surface (solid red line) and near bed (dashed blue line) temperatures at the centre of the stratified region namely (53.8°N, 5.5°W) with circles and diamonds representing observed surface and bottom temperatures. Also given are time series of computed temperature profiles determined with (a) mesh G3AX and (b) mesh G3AXWL.

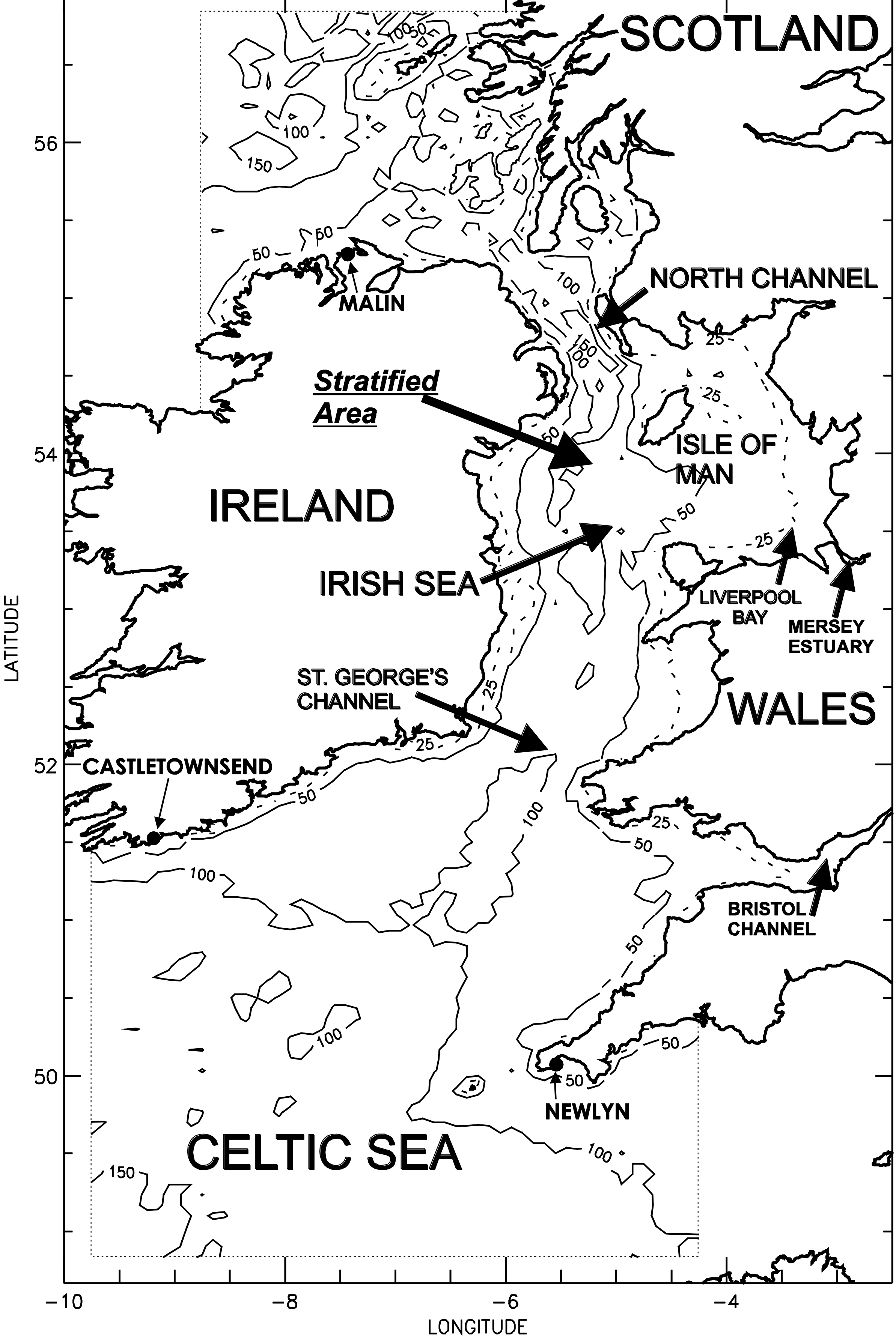
SCOTLAND
NORTH CHANNEL
MALIN
Stratified Area
IRELAND
ISLE OF MAN
IRISH SEA
LIVERPOOL BAY
MERSEY ESTUARY
ST. GEORGE'S CHANNEL
WALES
CASTLETOWNSEND
BRISTOL CHANNEL
NEWLYN
CELTIC SEA
LATITUDE
LONGITUDE
56
54
52
50
−10
−8
−6
−4
25
50
100
150

Fig 1

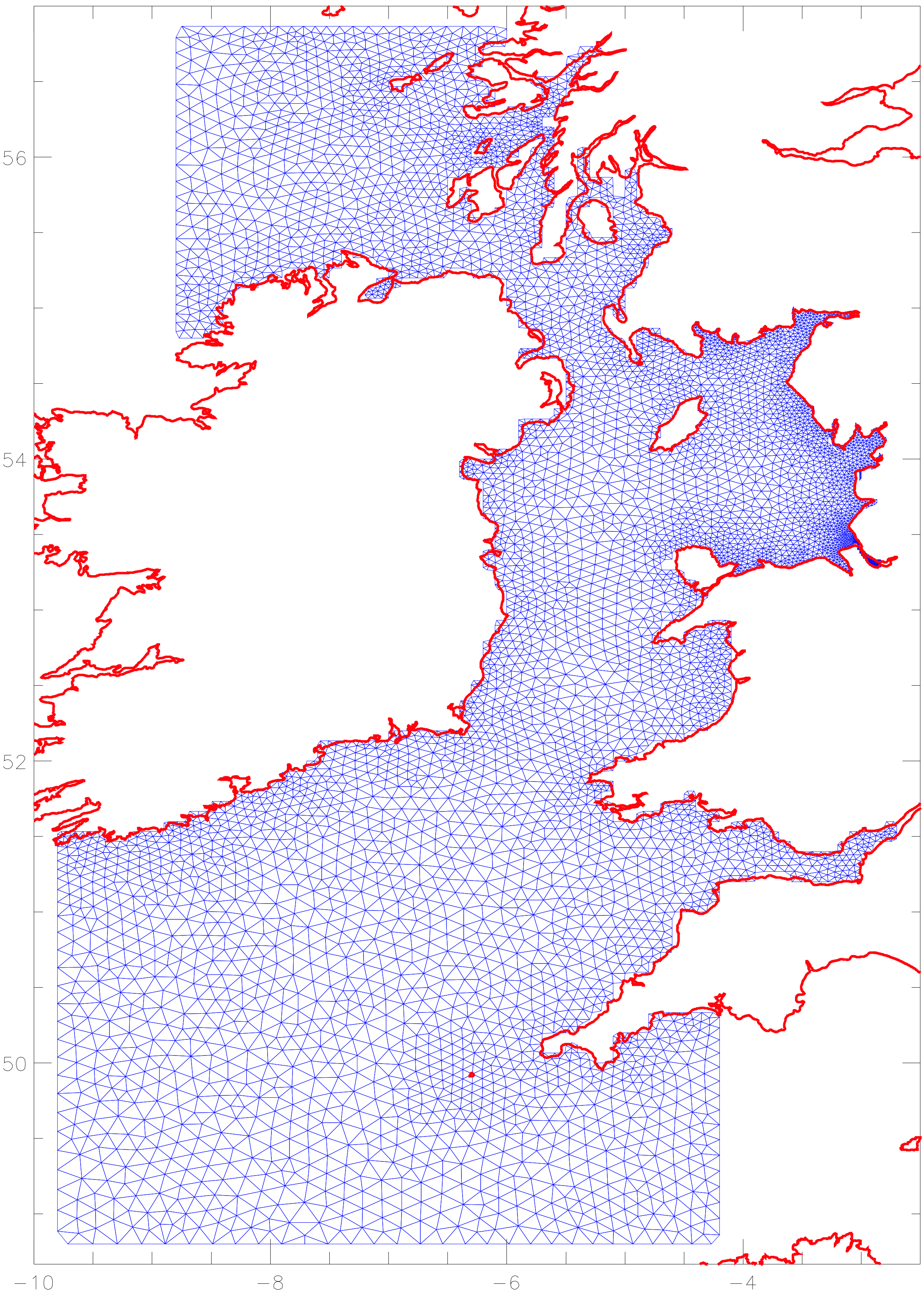

Fig 2a

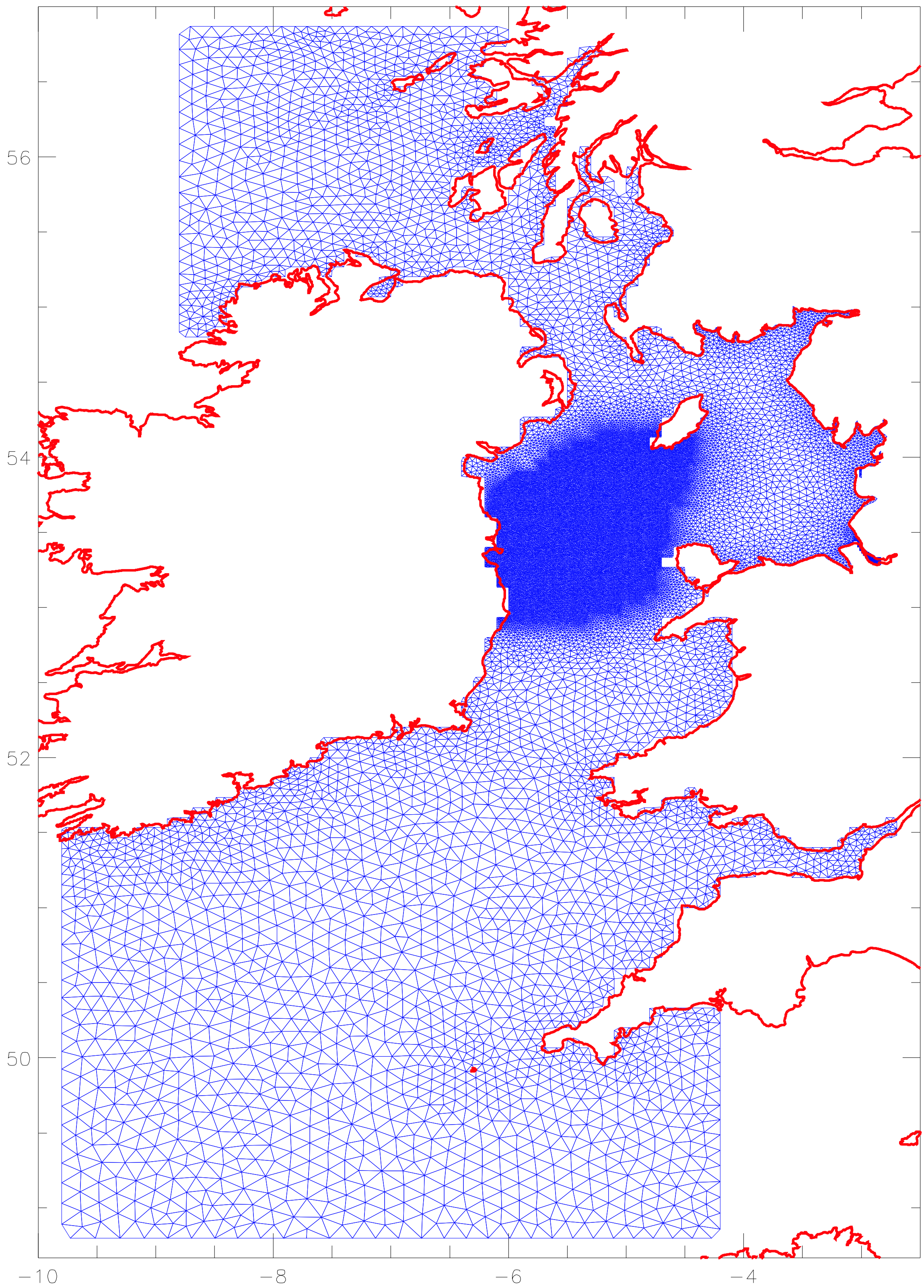

Fig 2b

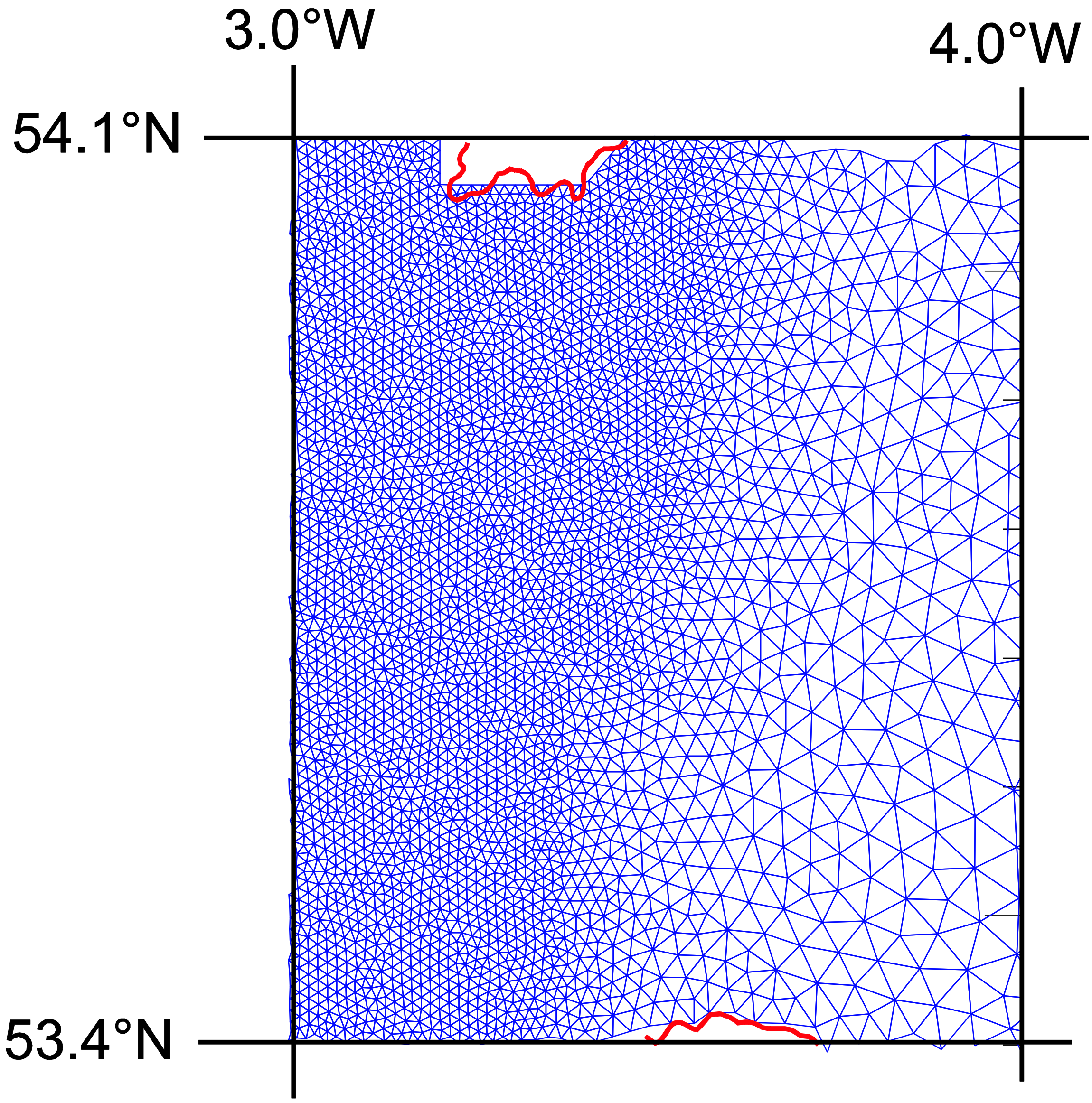

Fig 2c

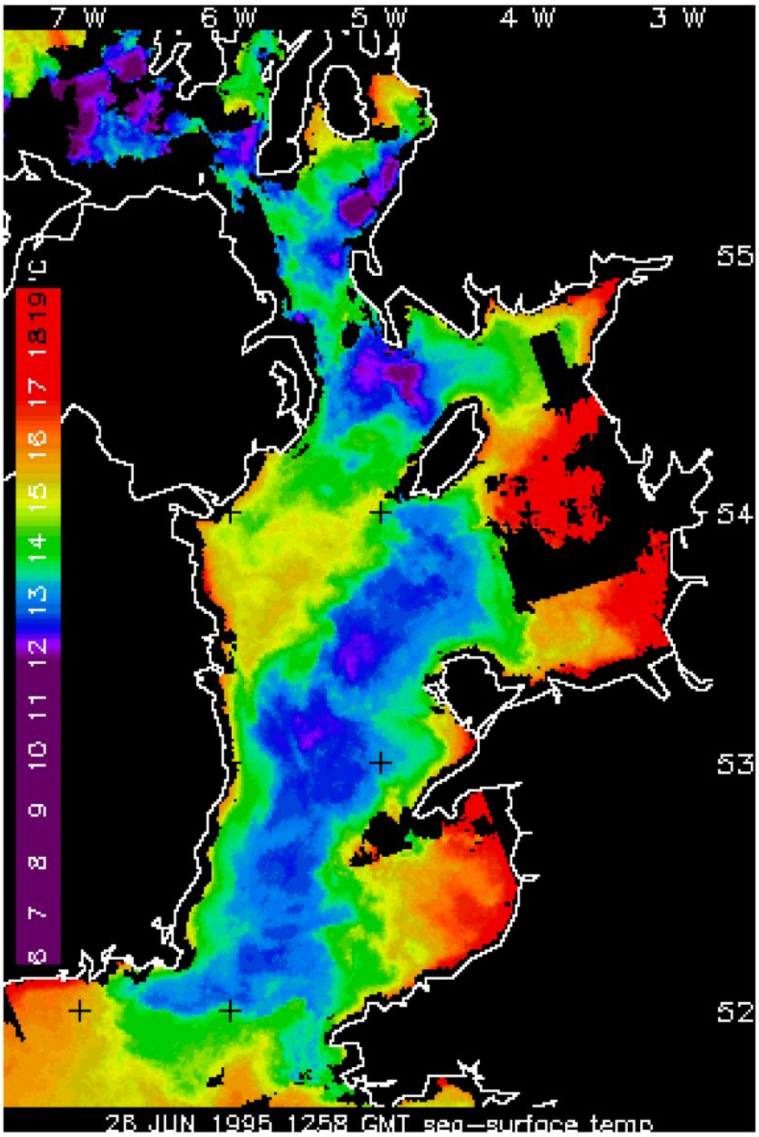

7 W
6 W
5 W
4 W
3 W
55
54
53
52
6 7 8 9 10 11 12 13 14 15 16 17 18 19 °C
28 JUN 1995 1258 GMT sea-surface temp

Fig 3

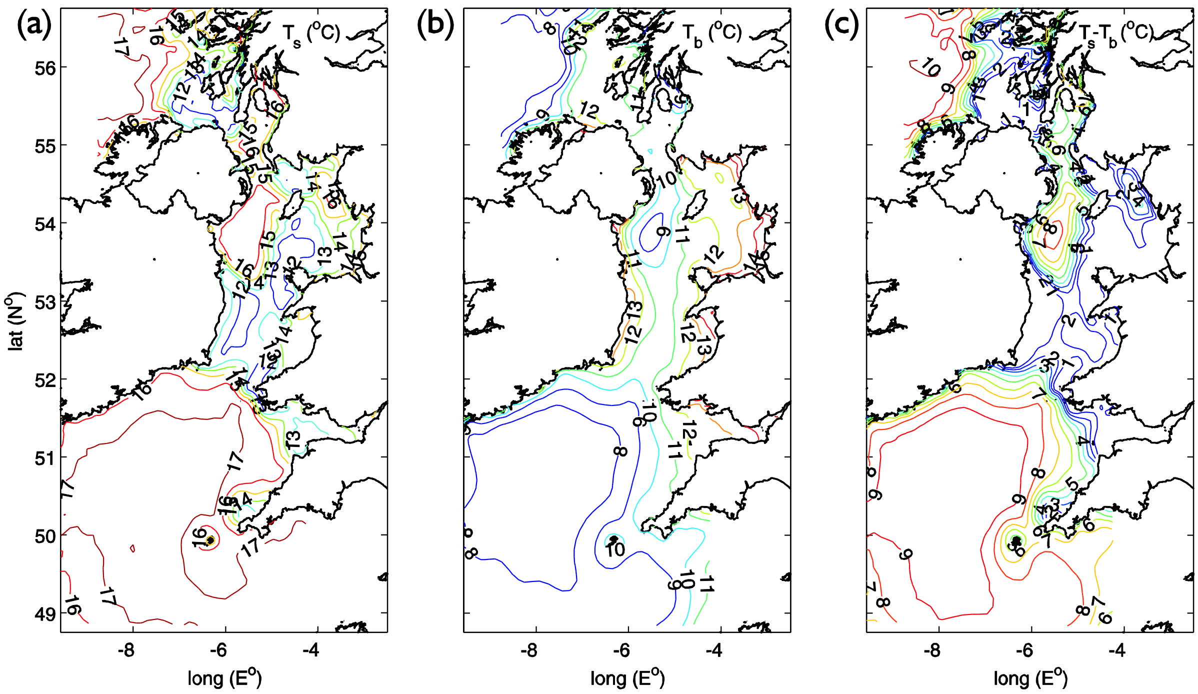

Fig 4a-c

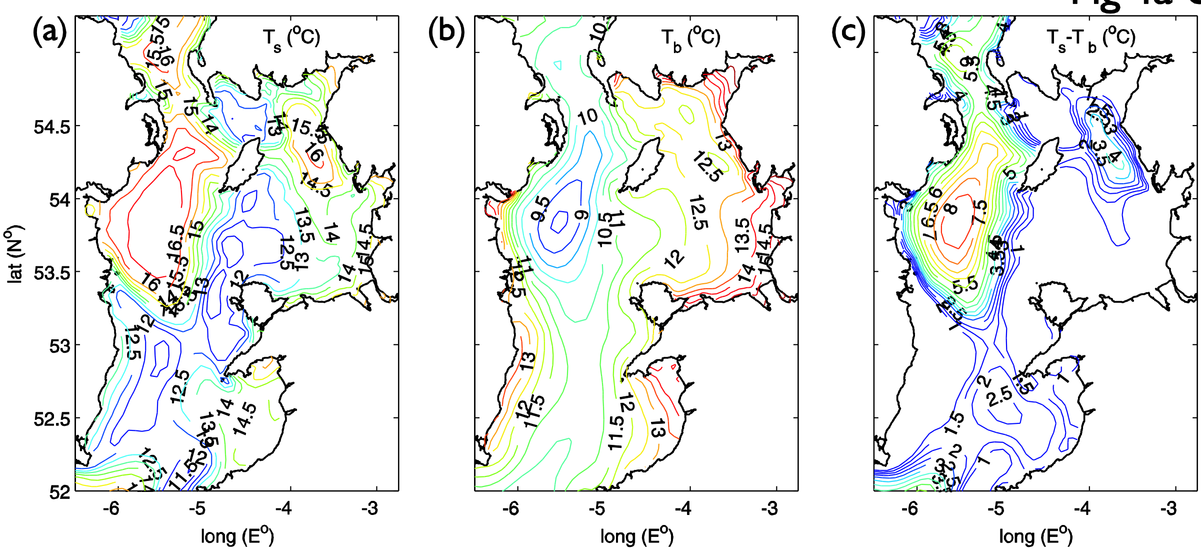

Fig 5a-c

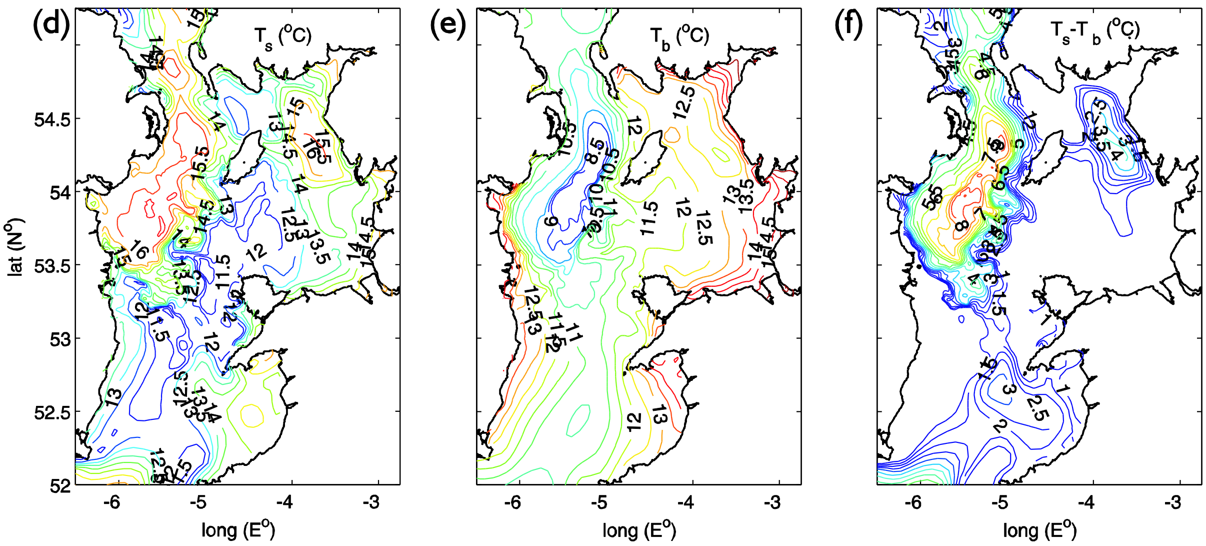

Fig 5d-f

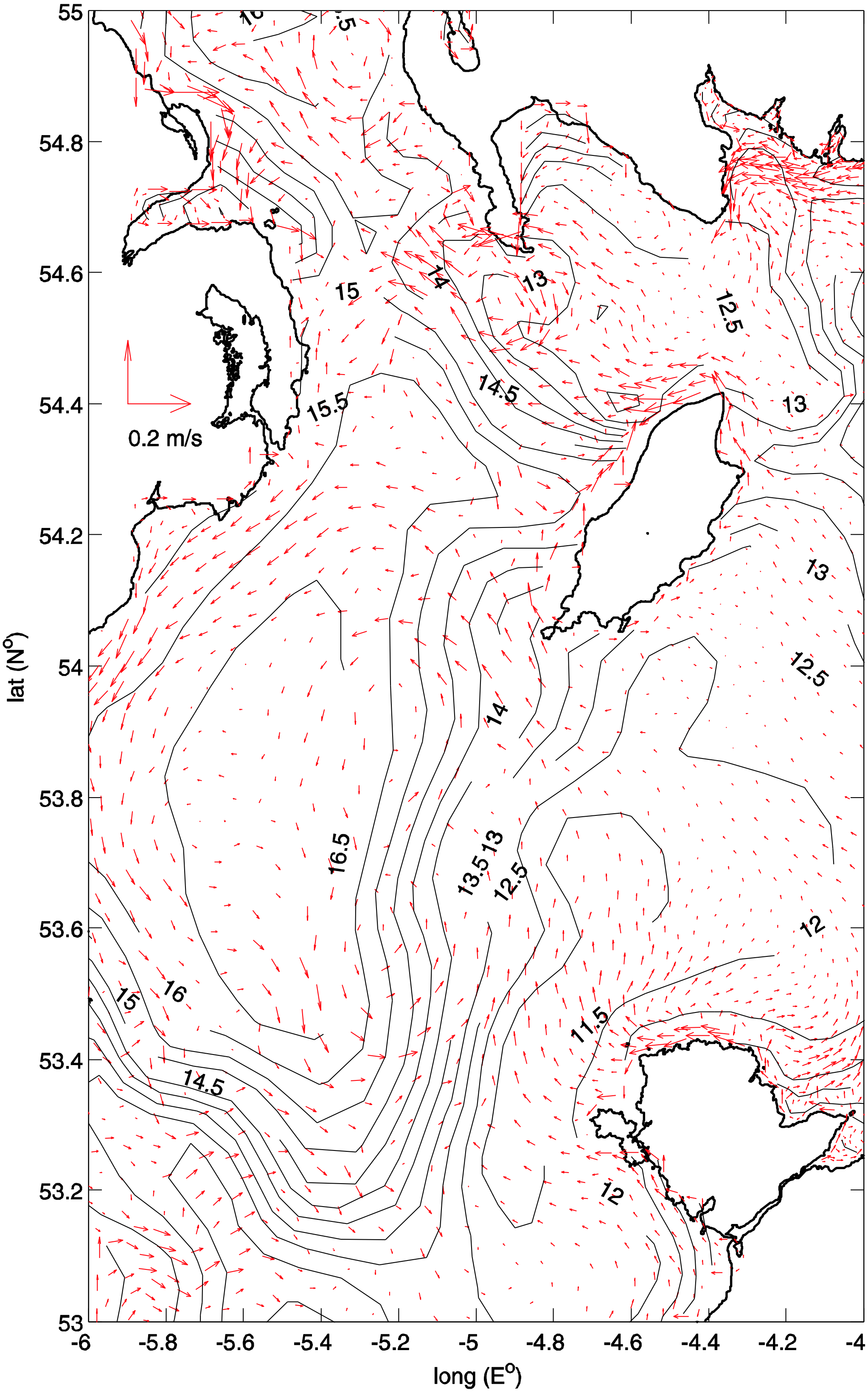

Fig 6a

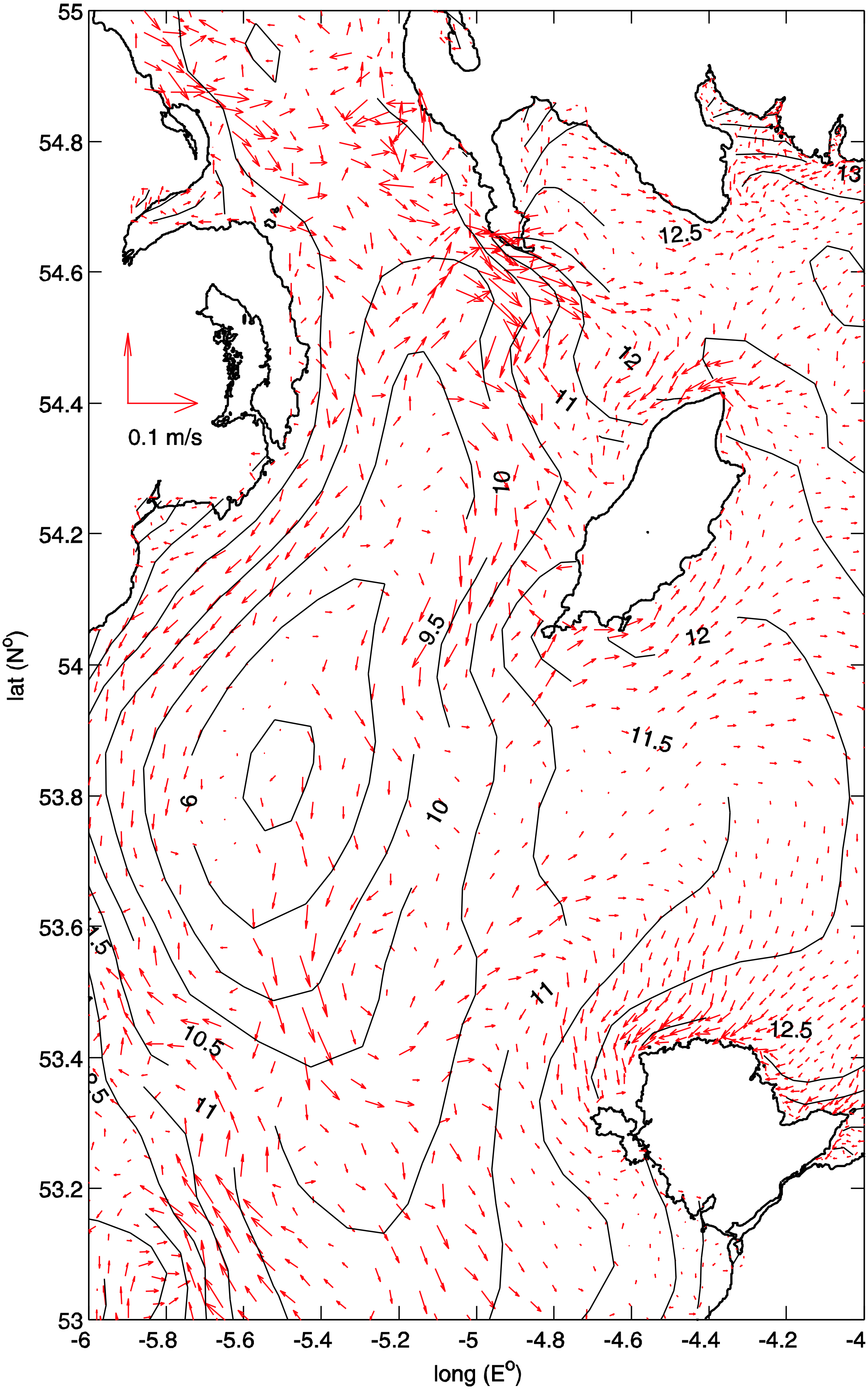

55
54.8
54.6
54.4
54.2
54
53.8
53.6
53.4
53.2
53
-6
-5.8
-5.6
-5.4
-5.2
-5
-4.8
-4.6
-4.4
-4.2
-4
lat (N°)
long (E°)
0.1 m/s
13
12.5
12
11
10
9.5
9
11.5
10
11
10.5
11
12.5

Fig 6b

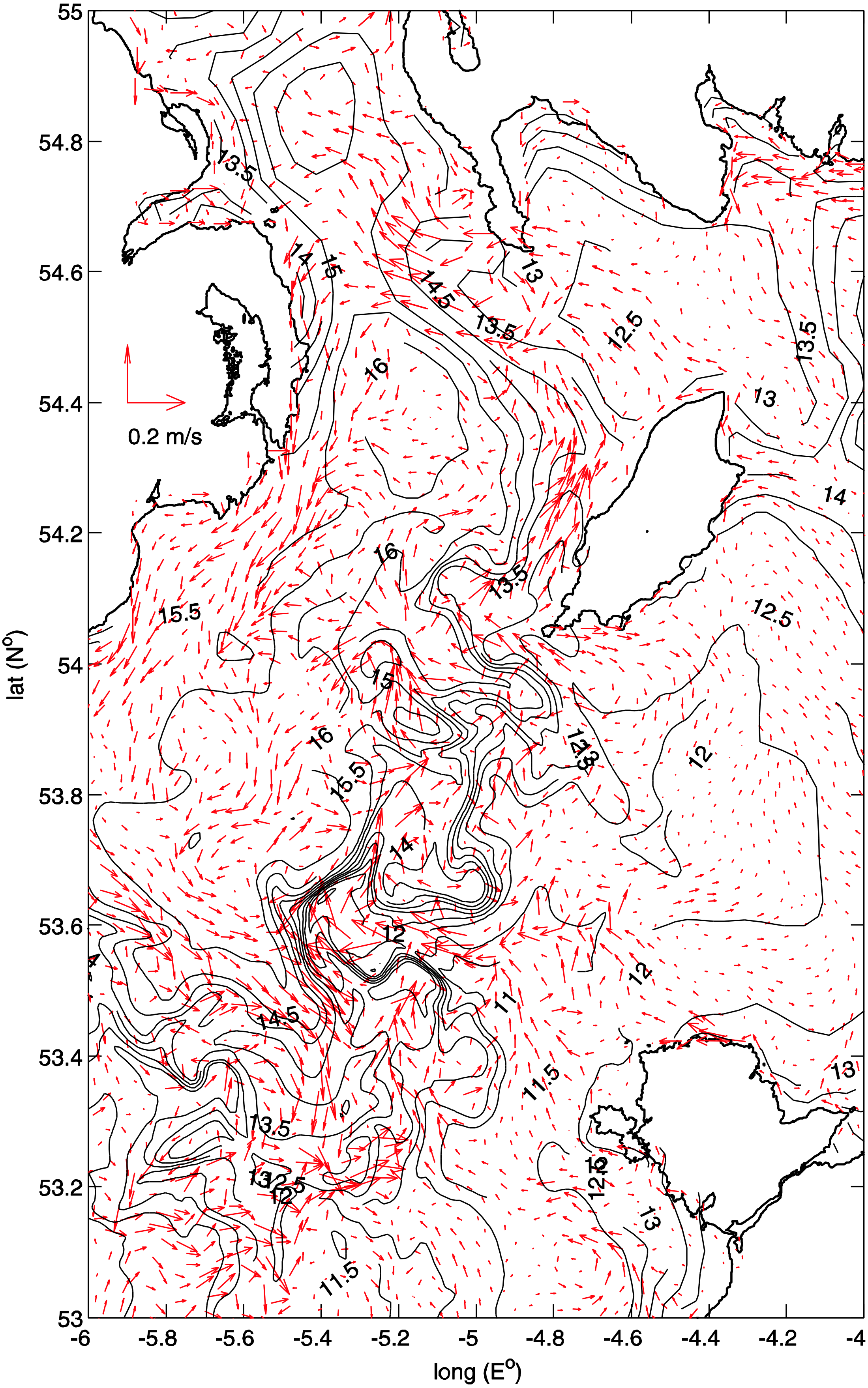

lat (N°)
long (E°)
0.2 m/s
55
54.8
54.6
54.4
54.2
54
53.8
53.6
53.4
53.2
53
-6
-5.8
-5.6
-5.4
-5.2
-5
-4.8
-4.6
-4.4
-4.2
-4
13.5
14
15
14.5
13.5
13
12.5
13.5
13
16
14
16
13.5
15.5
12.5
15
16
15.5
12
14
12
12
14.5
11
11.5
13.5
13
12.5
12
11.5
13

Fig 6c

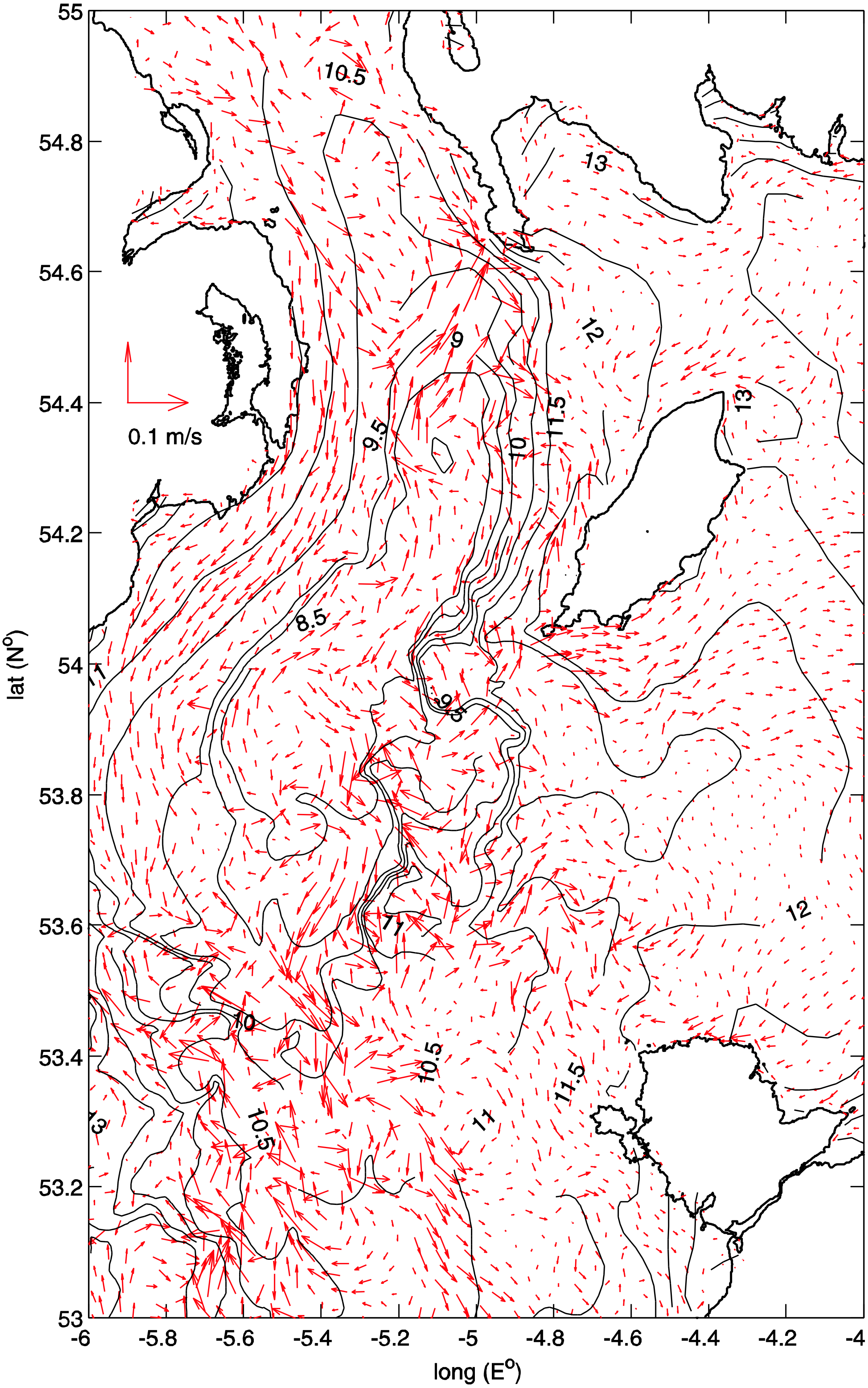

0.1 m/s
lat (N°)
long (E°)
55
54.8
54.6
54.4
54.2
54
53.8
53.6
53.4
53.2
53
-6
-5.8
-5.6
-5.4
-5.2
-5
-4.8
-4.6
-4.4
-4.2
-4

Fig 6d

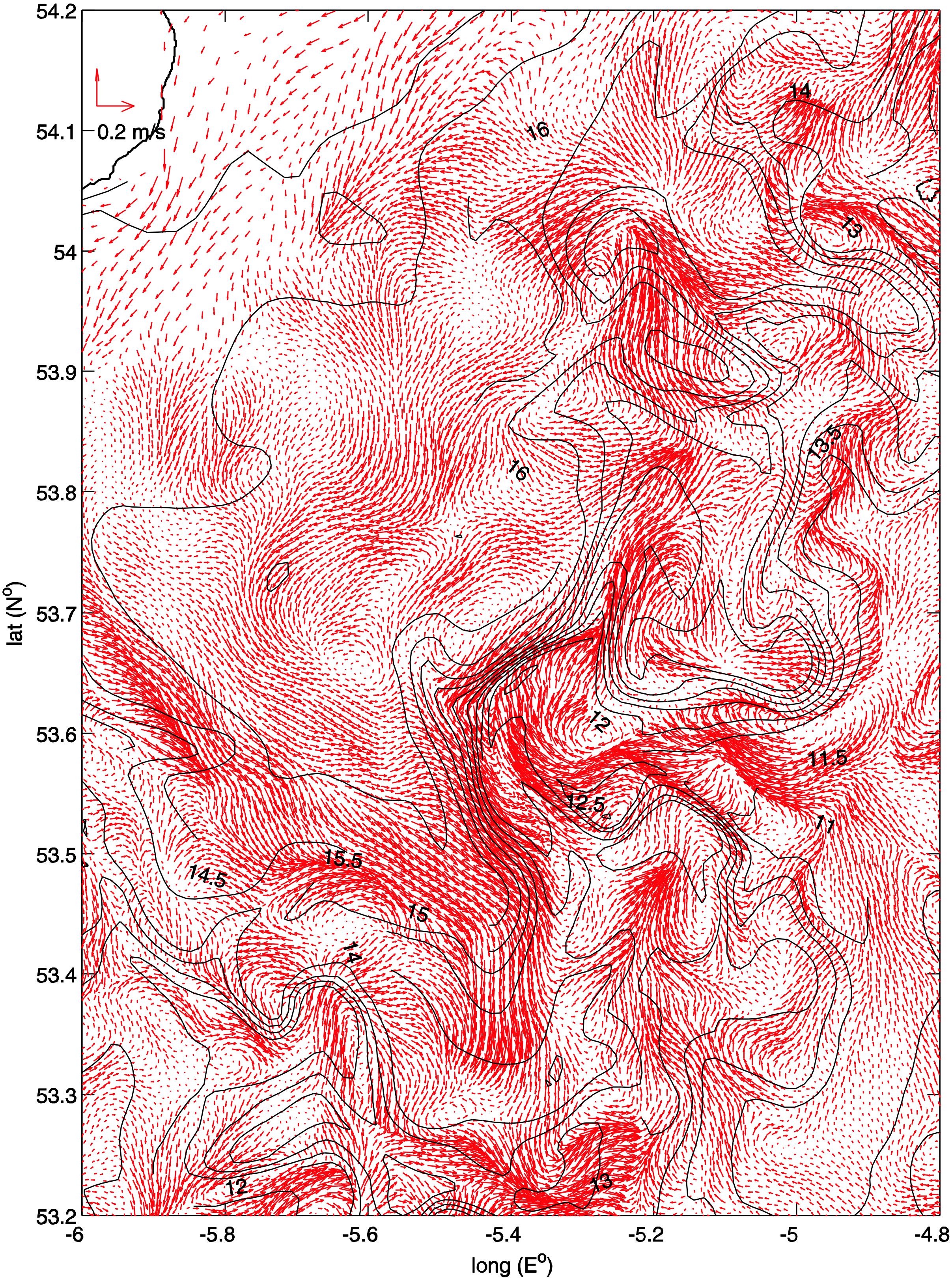

54.2
54.1
54
53.9
53.8
53.7
53.6
53.5
53.4
53.3
53.2
lat (N°)
-6
-5.8
-5.6
-5.4
-5.2
-5
-4.8
long (E°)
0.2 m/s
16
14
13
13.5
12
11.5
12.5
11
15.5
14.5
15

Fig 6e

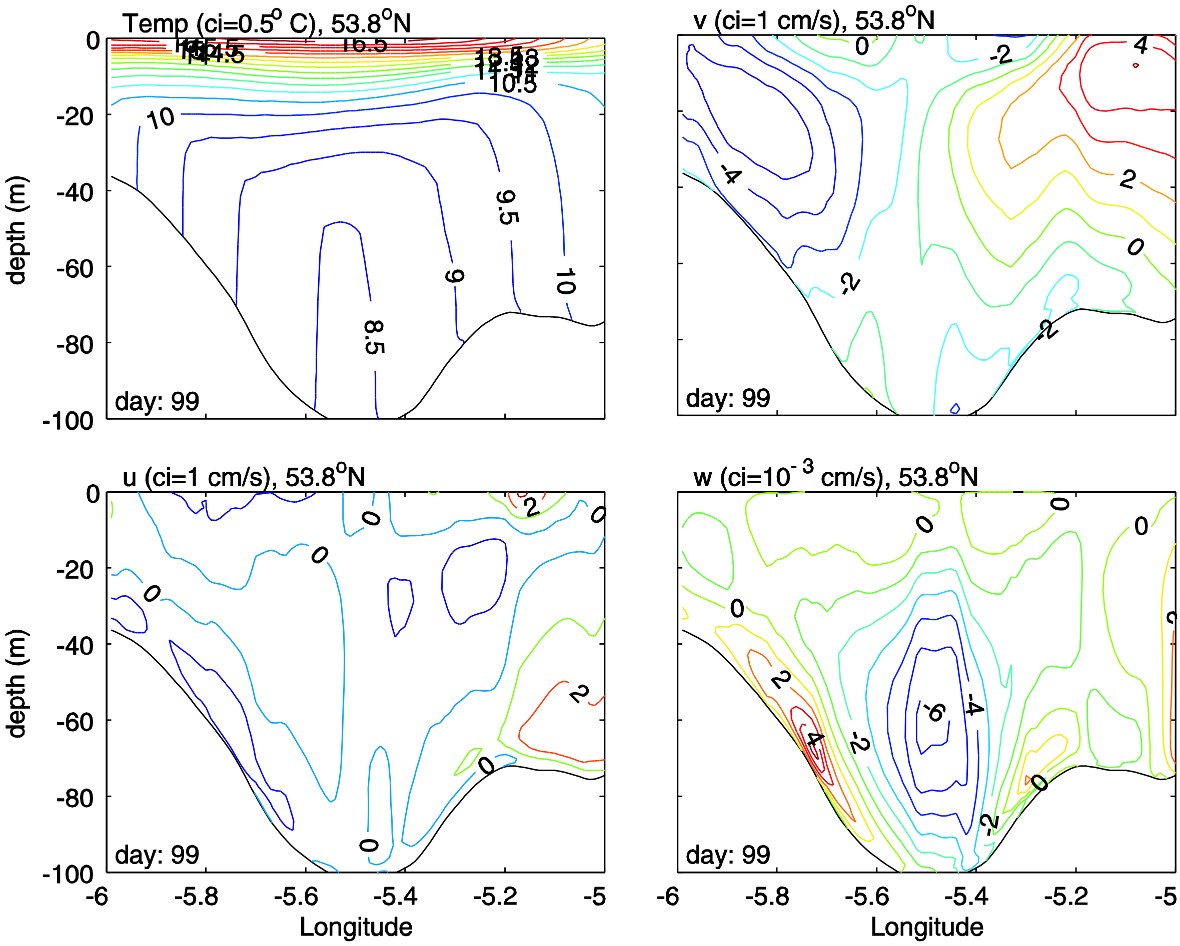

Temp (ci=0.5° C), 53.8°N
v (ci=1 cm/s), 53.8°N
u (ci=1 cm/s), 53.8°N
w (ci=10⁻³ cm/s), 53.8°N
depth (m)
Longitude
day: 99

Fig 7a

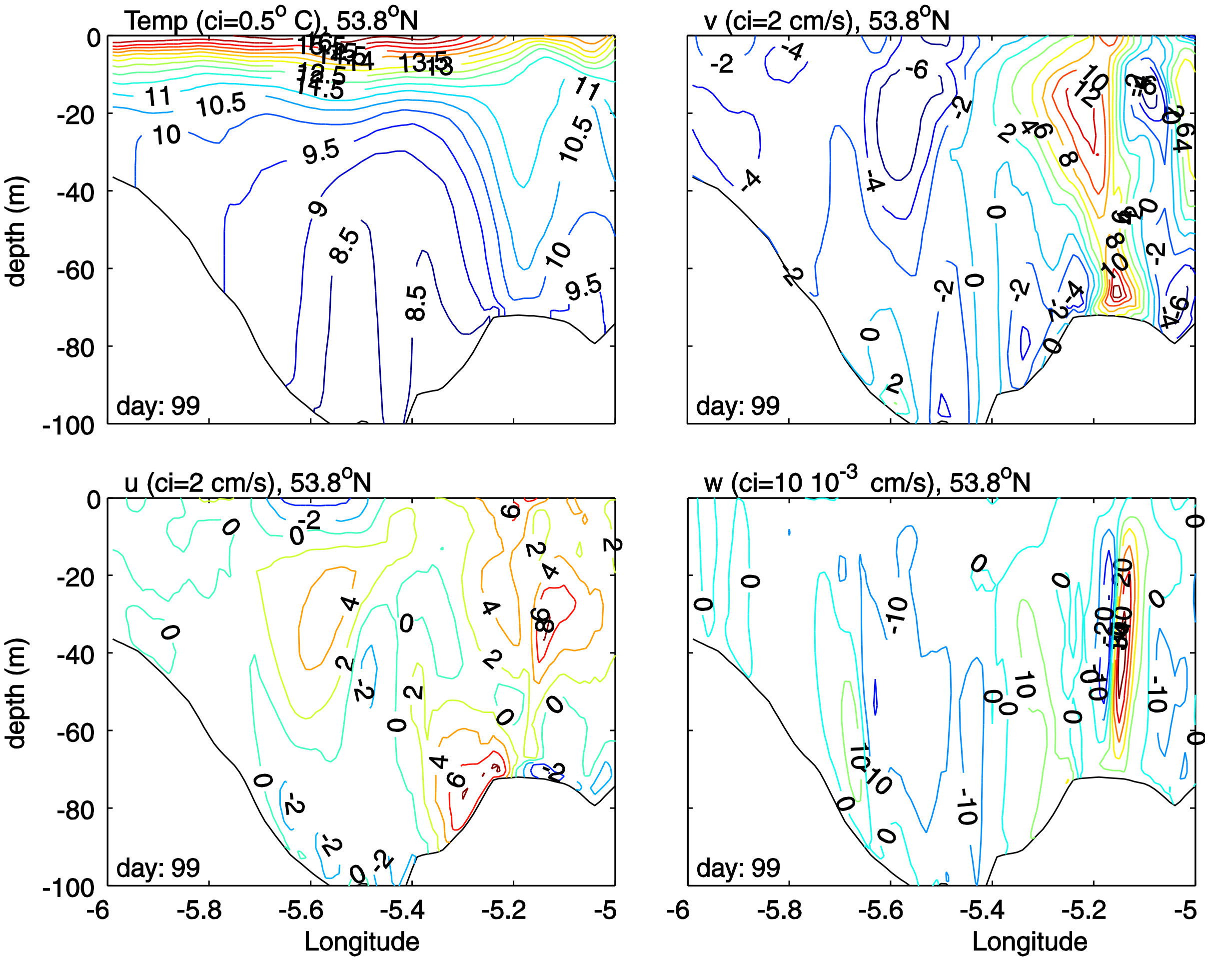

Fig 7b

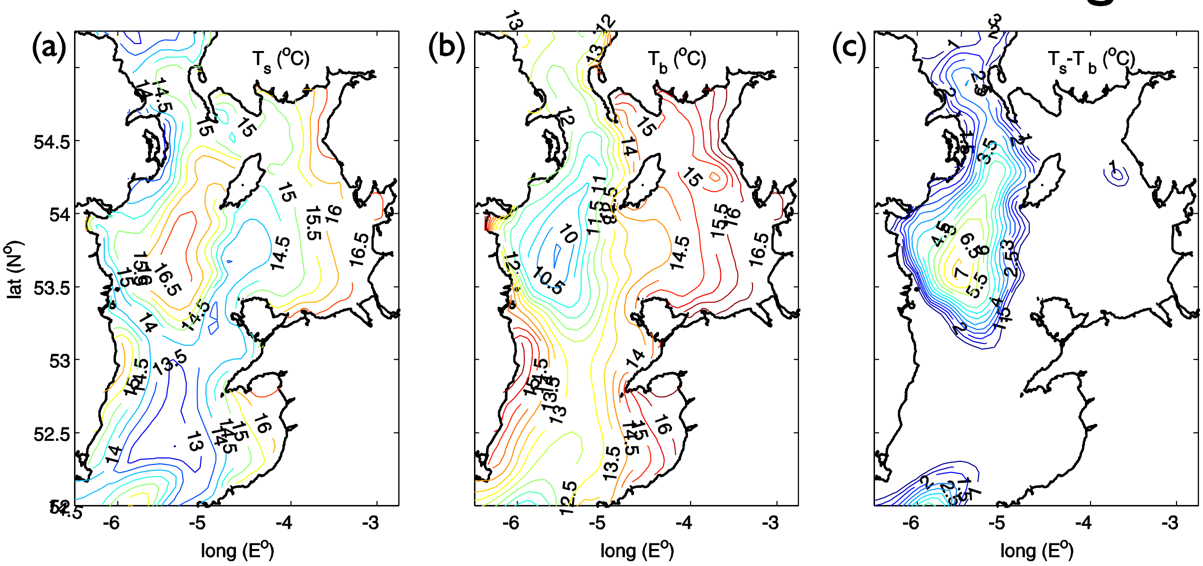

Fig 8a-c

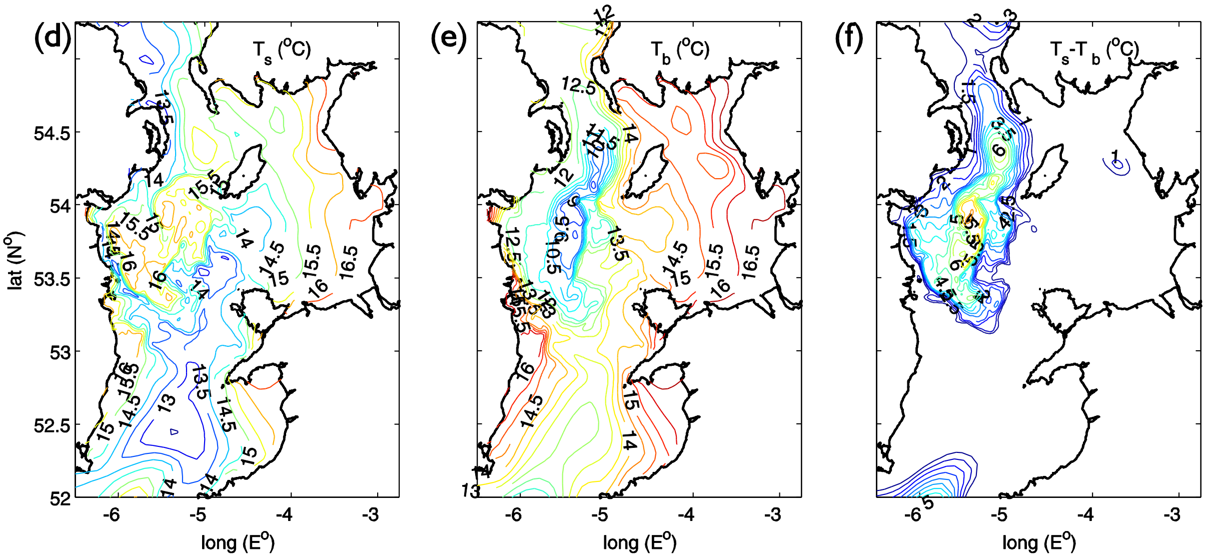

Fig 8d-f

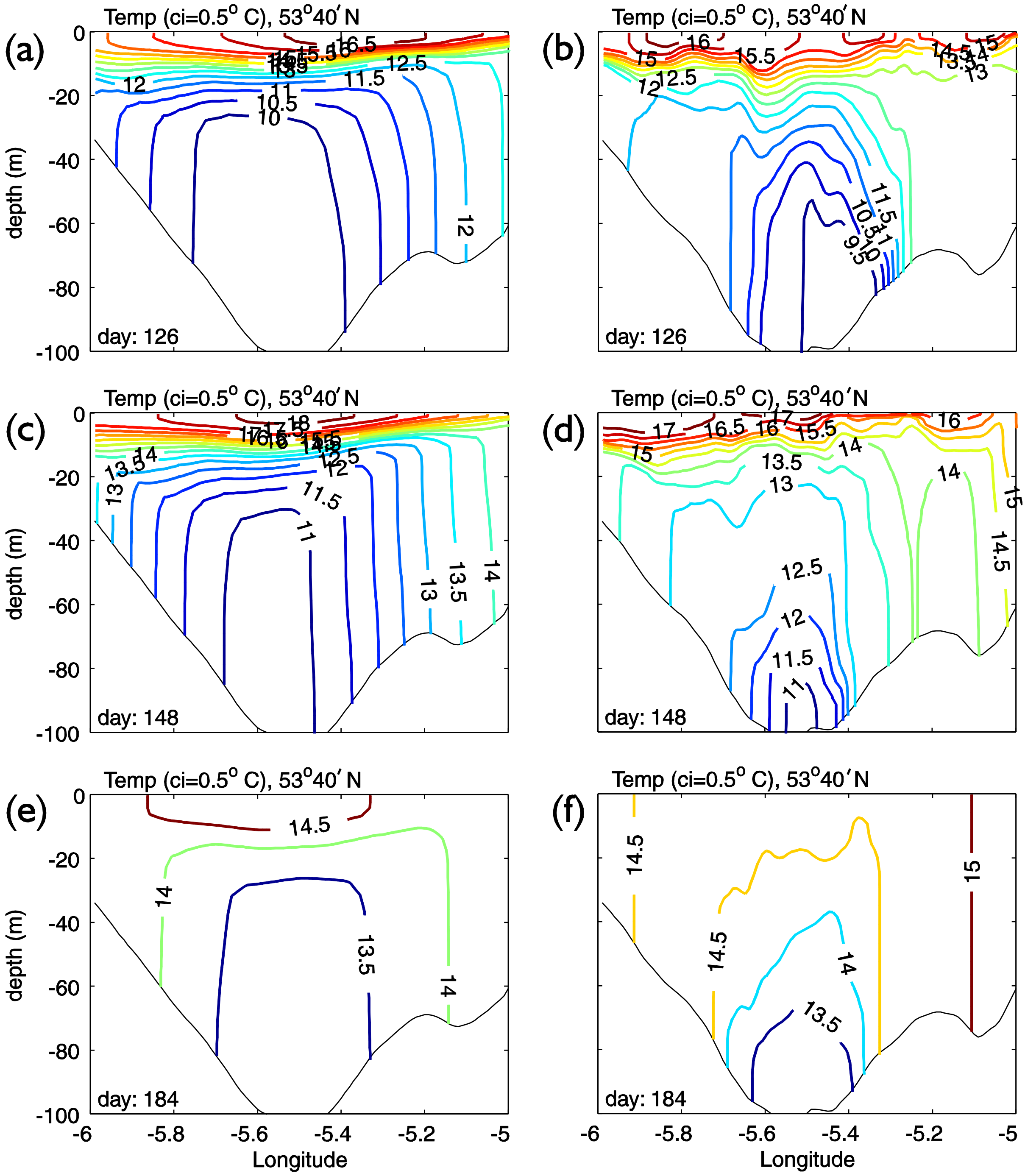

Temp (ci=0.5° C), 53°40′N
(a)
(b)
(c)
(d)
(e)
(f)
depth (m)
Longitude
day: 126
day: 148
day: 184

Fig 9a-f

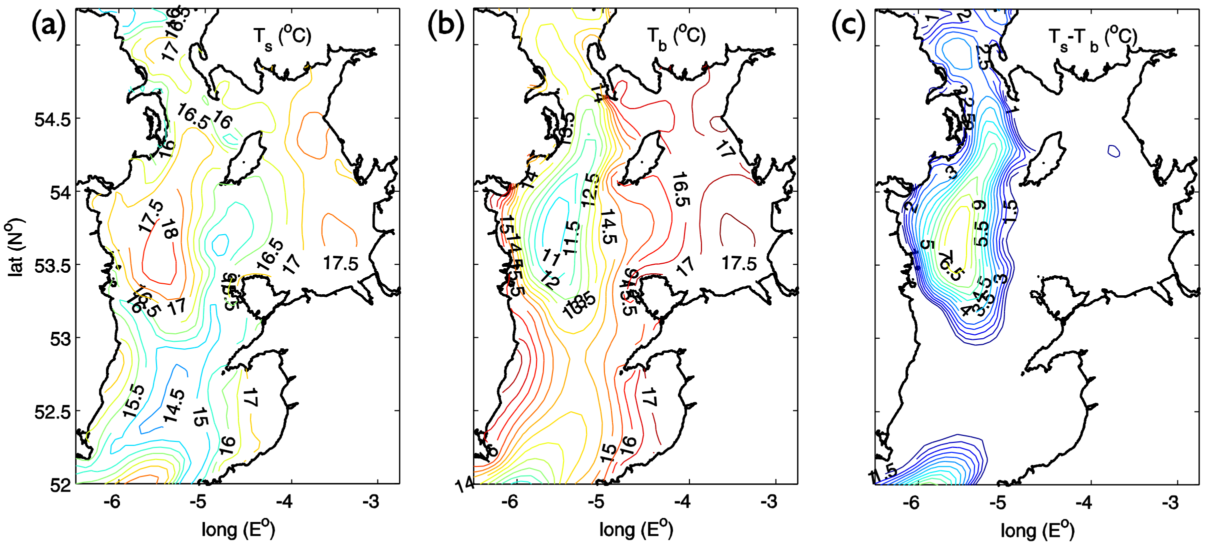

Fig 10a-c

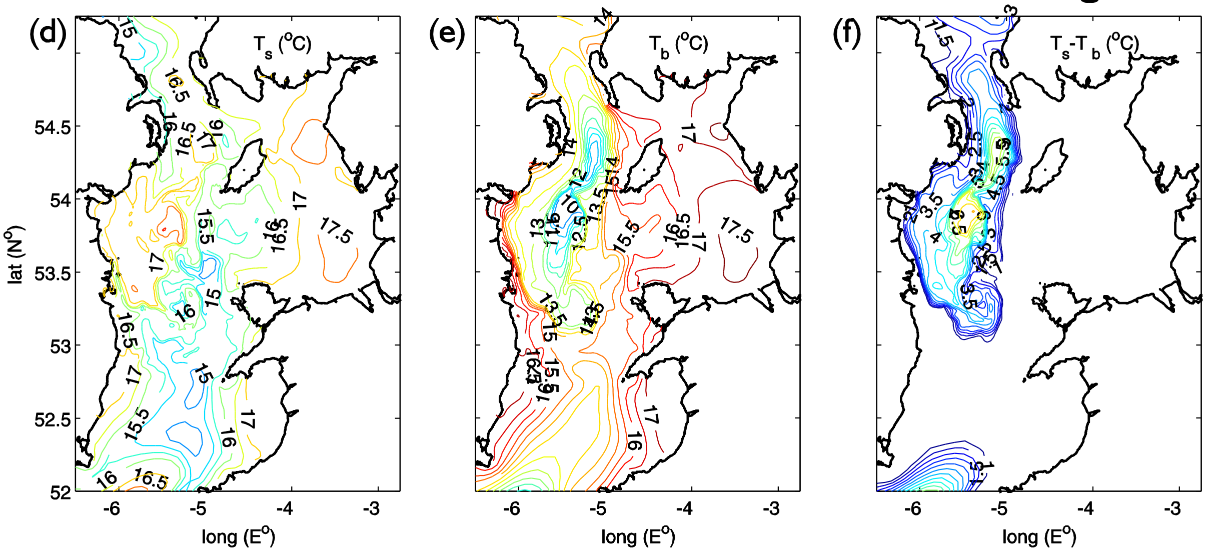

Fig 10d-f

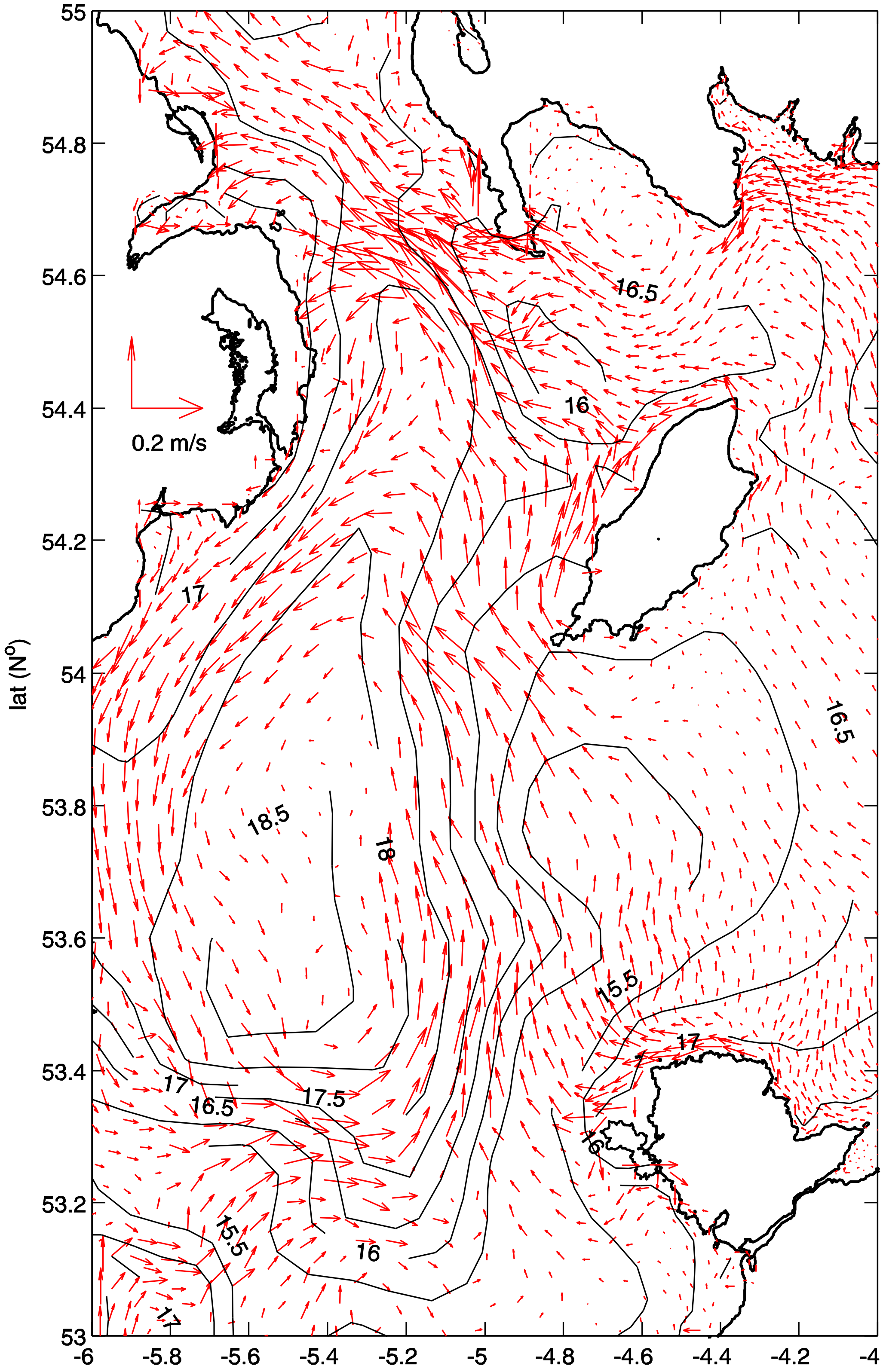

55
54.8
54.6
54.4
54.2
54
53.8
53.6
53.4
53.2
53
lat (N^o)
-6
-5.8
-5.6
-5.4
-5.2
-5
-4.8
-4.6
-4.4
-4.2
-4
long (E^o)
0.2 m/s
16.5
16
17
18.5
18
15.5
17
17
16.5
17.5
16
15.5
16
17
16.5

Fig 11a

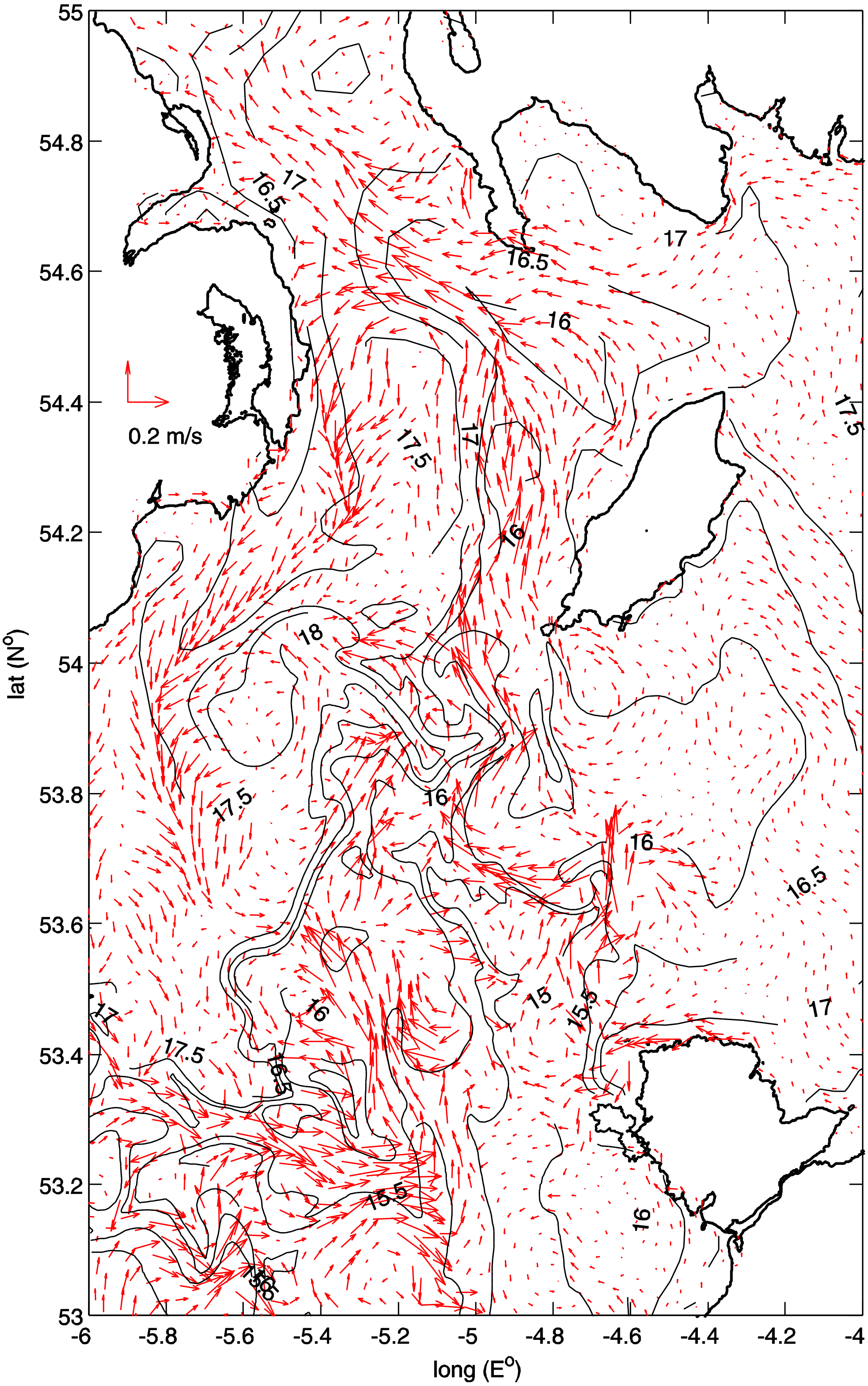

0.2 m/s
lat (N°)
long (E°)
55
54.8
54.6
54.4
54.2
54
53.8
53.6
53.4
53.2
53
-6
-5.8
-5.6
-5.4
-5.2
-5
-4.8
-4.6
-4.4
-4.2
-4

Fig 11b

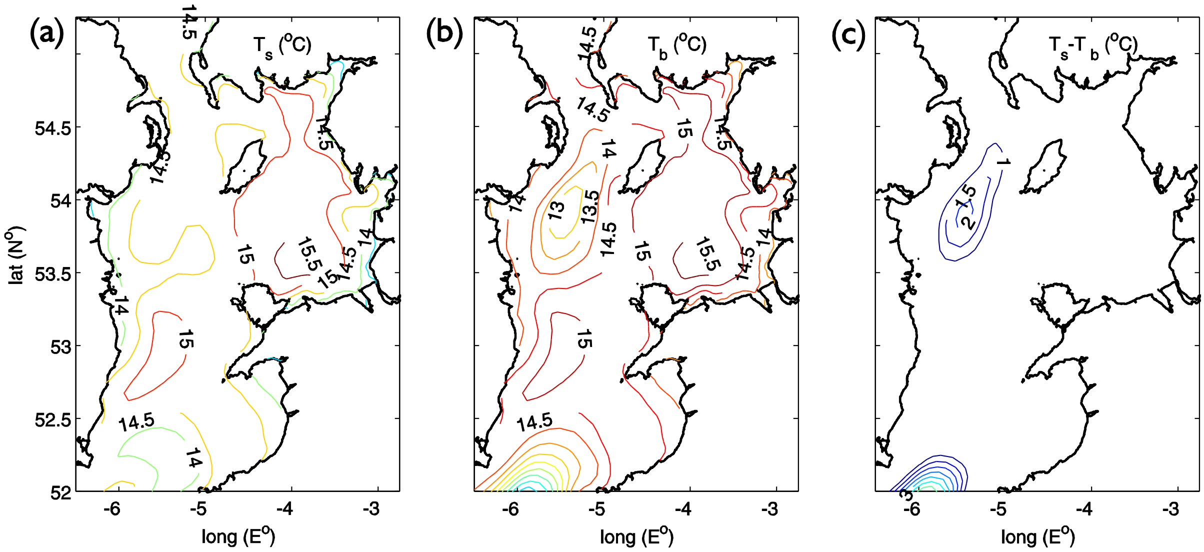

Fig 12a-c

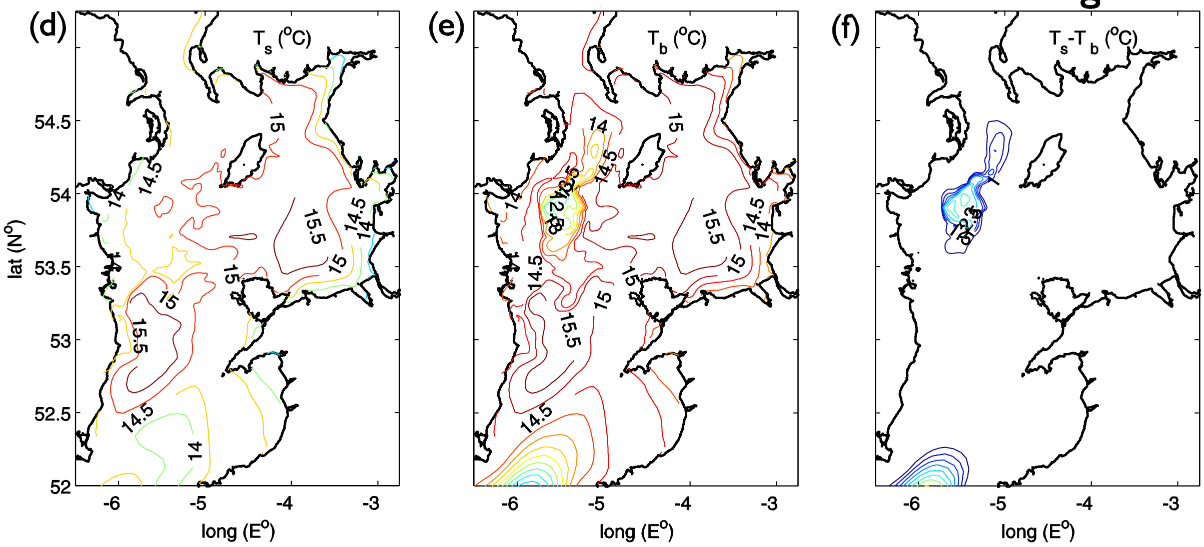

Fig 12d-f

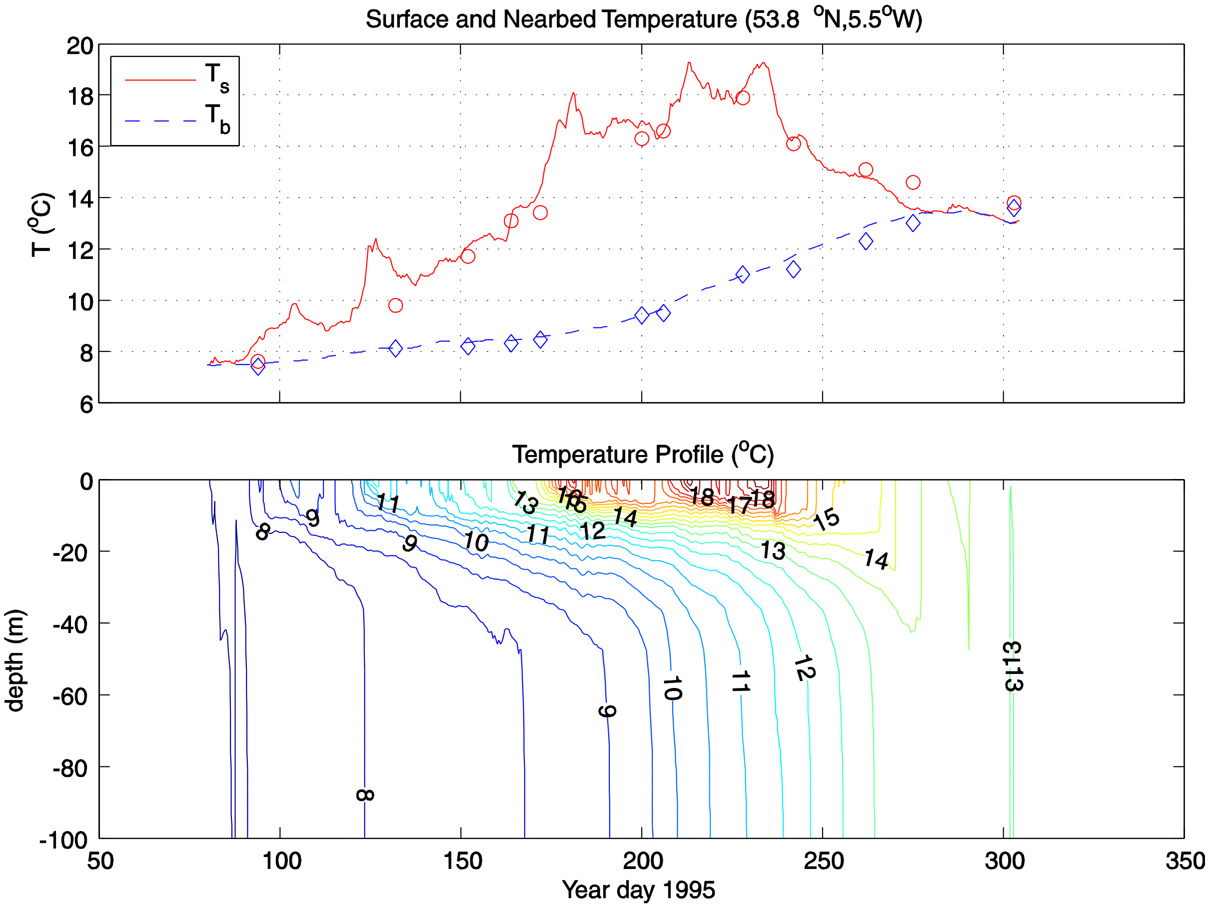

Surface and Nearbed Temperature (53.8 °N,5.5°W)
T (°C)
Ts
Tb
Temperature Profile (°C)
depth (m)
Year day 1995

Fig 13a

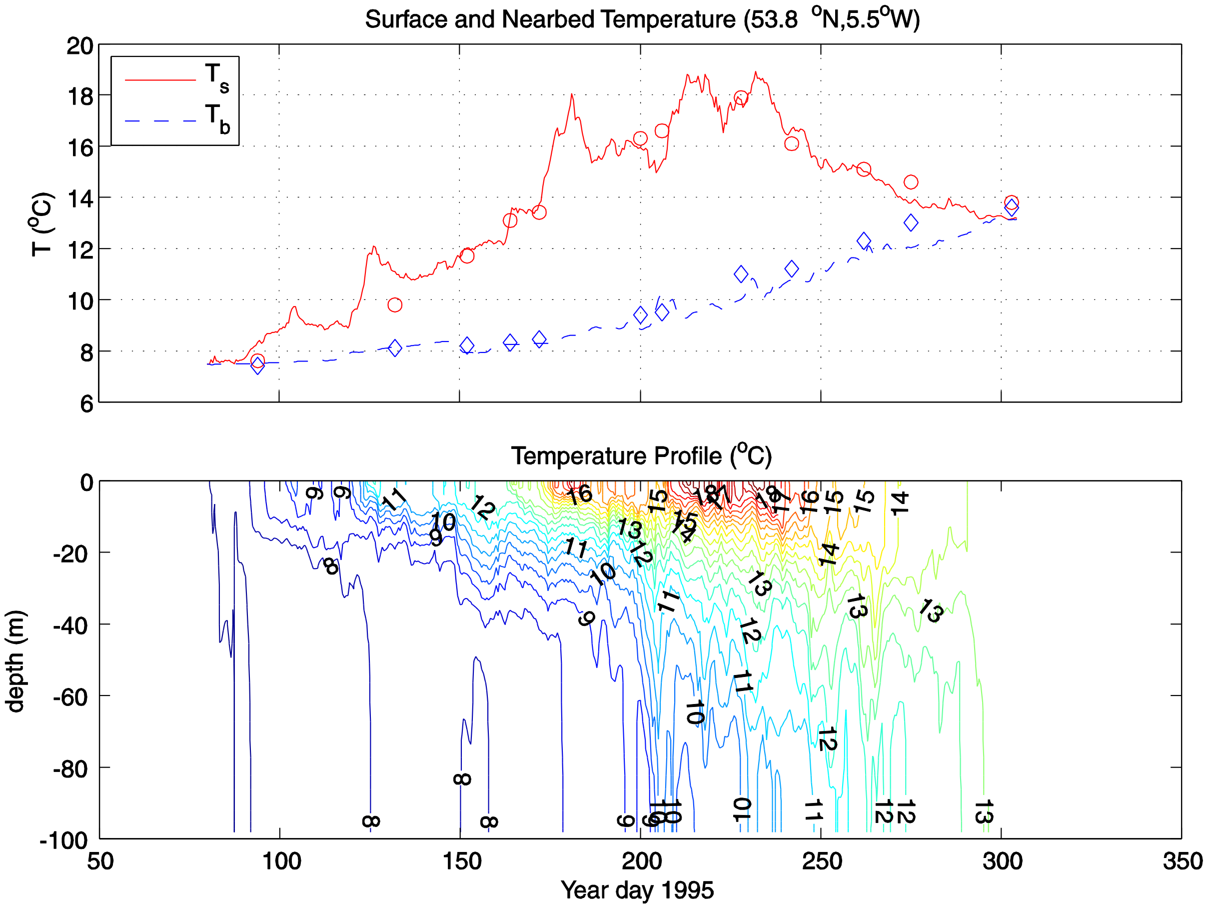

Surface and Nearbed Temperature (53.8 °N,5.5°W)
T (°C)
Ts
Tb
Temperature Profile (°C)
depth (m)
Year day 1995

Fig 13b